

Garlic-Derived Exosome-Like Nanovesicles: A Promising Natural Nanotherapy for Periodontitis via PHGDH/PI3K/AKT-Mediated Metabolic and Inflammatory Regulation

Chenhao Yu¹, Yuanqing Liu¹, Xiaotong Yu², Jia Liu¹, Pei Cao¹, Guojing Liu¹, Yu Cai¹, Yong Zhang¹, Qingxian Luan¹ 

¹Department of Periodontology, Peking University School and Hospital of Stomatology & National Center for Stomatology & National Clinical Research Center for Oral Diseases & National Engineering Research Center of Oral Biomaterials and Digital Medical Devices & Beijing Key Laboratory of Digital Stomatology & NHC Key Laboratory of Digital Stomatology & NMPA Key Laboratory for Dental Materials, Beijing, 100081, People's Republic of China; ²Department of Orthodontics, Peking University School and Hospital of Stomatology & National Center for Stomatology & National Clinical Research Center for Oral Diseases & National Engineering Laboratory for Digital and Material Technology of Stomatology & Beijing Key Laboratory of Digital Stomatology & Research Center of Engineering and Technology for Computerized Dentistry Ministry of Health & NMPA Key Laboratory for Dental Materials, Beijing, People's Republic of China

Correspondence: Qingxian Luan, Email kqluanqx@bjmu.edu.cn

Background: Periodontitis is a chronic inflammatory disease that leads to alveolar bone loss, with a complex pathogenesis closely associated with excessive local inflammation and metabolic dysregulation in periodontal tissues. Unfortunately, effective therapeutic strategies targeting inflammation and improving cellular metabolism remain lacking. Garlic-derived exosome-like nanovesicles (GaELNs), as a natural therapeutic agent, have demonstrated significant therapeutic effects in conditions such as colitis, liver dysfunction, osteoarthritis, and adipose tissue inflammation, yet their potential in treating periodontitis has not been explored.

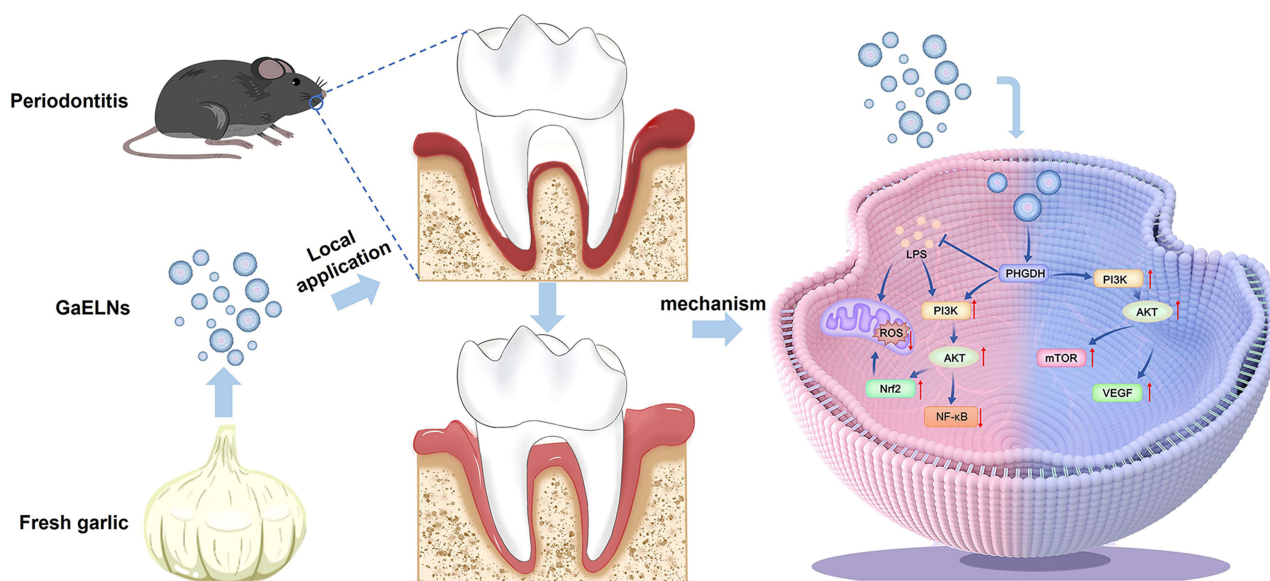
Methods: In this study, GaELNs were extracted using a simplified and rapid method and characterized for their morphology and concentration. Metabolomic analysis was conducted to determine the bioactive components within GaELNs. In vitro experiments using human gingival fibroblasts assessed GaELNs' cellular uptake, effects on cell proliferation, migration, VEGF expression, and their ability to attenuate lipopolysaccharide-induced oxidative stress and pro-inflammatory cytokine expression. Additionally, a mouse periodontitis model was employed to evaluate the in vivo effects of GaELNs on local inflammation and bone resorption.

Results: GaELNs exhibited typical exosome-like characteristics with sufficient concentration and high batch-to-batch reproducibility. Metabolomic analysis revealed that GaELNs are enriched with bioactive components possessing anti-inflammatory, antioxidative, and regenerative properties. In vitro, GaELNs were efficiently internalized by human gingival fibroblasts, significantly enhancing their proliferation, migration, and VEGF expression, while markedly reducing LPS-induced oxidative stress and pro-inflammatory factor expression. In the mouse periodontitis model, local administration of GaELNs significantly reduced gingival inflammation and alveolar bone resorption. These therapeutic effects were mediated by upregulation of PHGDH, activation of the PI3K/AKT signaling pathway, increased expression of mTOR and Nrf2, and inhibition of NF- κ B activity, which together contributed to improved mitochondrial function and metabolic reprogramming under inflammatory conditions.

Conclusion: GaELNs demonstrate potent anti-inflammatory, antioxidative, and metabolism-enhancing properties, offering significant therapeutic potential for the treatment of periodontitis by modulating the PHGDH/PI3K/AKT pathway.

Plain Language Summary: Dr Luan's team report that garlic-derived exosome-like nanovesicles (GaELNs) can reduce inflammation, oxidative stress, and damage to mitochondria by activating a specific cell signaling pathway known as PHGDH/PI3K/AKT. This process helps prevent tissue damage caused by periodontitis, a common gum disease. GaELNs offer a promising natural treatment to protect against periodontal tissue loss and improve oral health, making them an exciting option for future therapies.

Graphical Abstract



GaELNs alleviate cellular inflammation, oxidative stress and mitochondrial dysfunction by activating the PHGDH/PI3K/AKT pathway, thereby mitigating tissue loss associated with periodontitis.

Keywords: garlic-derived exosome-like nanovesicles, periodontitis, PHGDH, PI3K/AKT, mitochondria

Introduction

Periodontitis is a chronic inflammatory disease induced by bacterial infection, with its pathogenesis closely associated with metabolic dysregulation and inflammatory responses.^{1–3} As a primary component of periodontal tissue, gingival fibroblasts are the first to detect bacterial accumulation and initiate a localized inflammatory response through the secretion of inflammatory mediators and cytokines.^{4–6} Under sustained infection and inflammatory stimuli, mitochondrial metabolism becomes impaired, causing a shift from aerobic metabolism to glycolysis. This shift provides rapid energy in the short term, supporting the ongoing inflammatory response.^{7–9} Concurrently, mitochondrial dysfunction leads to the accumulation of reactive oxygen species (ROS).¹⁰ When glycolytic metabolites and ROS reach a decompensated level, the inflammatory response becomes uncontrolled, osteoclast activity increases and alveolar bone resorption occurs, resulting in periodontal tissue destruction.¹¹

The interplay between metabolic dysregulation and inflammatory responses renders periodontitis a complex, metabolism-associated chronic disease. The PI3K/AKT signaling pathway plays a crucial role in this process, acting as a double-edged sword. It can activate downstream pathways, such as Nrf2 and mTOR, which mitigate oxidative stress, promote immune cell proliferation to clear pathogens, and support tissue repair and regeneration during the resolution phase of inflammation.^{12,13} However, it can also activate the NF-κB pathway, leading to excessive glycolytic metabolism, thereby sustaining and exacerbating inflammation.¹⁴ This escalation results in increased cell death and substantial destruction of periodontal tissues. Therefore, restoring normal cellular metabolism and reducing inflammatory responses offer promising strategies for treating periodontitis. However, the primary non-surgical treatments for periodontitis currently remain mechanical debridement combined with localized or systemic antibiotic administration, an approach that is far from satisfactory and poses risks such as antibiotic overuse and bacterial resistance. Therefore, it is crucial to develop strategies that directly suppress inflammation and improve the metabolic function of periodontal tissues.^{15,16}

Plant-derived exosome-like nanovesicles are nanoscale vesicles isolated from plant cells that contain various bioactive substances.^{17,18} Compared to animal-derived exosome-like nanovesicles, plant-derived nanovesicles are cost-effective and easier to produce.¹⁹ Plant-derived exosome-like nanovesicles also demonstrate higher safety profiles, making them more readily accepted by regulatory agencies and patients.^{20–22} Garlic, beyond its widespread use as a culinary spice, is recognized for its potential in preventing and treating various diseases. Previous studies have demonstrated that garlic and its extracts possess anti-cancer, antioxidant, anti-inflammatory and antibacterial properties, establishing it as a key therapeutic agent in both traditional and modern medicine.^{23–25} Furthermore, GaELNs have been shown to significantly reduce the secretion of inflammatory factors, inhibit the NF- κ B pathway and alleviate cellular oxidative stress, thereby demonstrating substantial therapeutic effects on conditions such as colitis²⁶, liver dysfunction,²⁷ osteoarthritis²⁸ and inflammation in adipose tissue.²⁹ However, their potential application in the field of periodontitis remains unexplored.

The significance of exploring natural therapeutic agents for disease treatment is profound. Therefore, the main objective of this study is to extract natural GaELNs using a simple, contamination-free method and to characterize their biological properties, including morphology, size, and protein distribution. Metabolomic approaches are then employed to identify the bioactive components of GaELNs, analyze their potential biological effects, and investigate the signaling pathways involved. Further, the study explores whether GaELNs can induce metabolic reprogramming to mitigate cellular inflammatory responses, reduce excessive oxidative stress, and restore mitochondrial function under lipopolysaccharide (LPS) stimulation. Simultaneously, the impact of GaELNs on inflammatory bone loss is assessed in a ligature-induced murine periodontitis model. This research provides valuable insights and support for the development of novel natural therapeutic agents and strategies for treating periodontitis.

Materials and Methods

Antibody

The following antibodies were used for WB or immunofluorescence labeling: HO-1 Rabbit mAb (A21911), Nrf2 Rabbit mAb (A21176), NQO1 Rabbit mAb (A23486), GAPDH Rabbit mAb (A19056), PHGDH Rabbit mAb (A22129), mTOR Rabbit pAb (A2445), NF- κ B p65 Rabbit mAb (A19653), TOM20 Rabbit mAb (A19403), TFAM Rabbit mAb (A3173), FITC-conjugated Goat anti-Rabbit IgG (AS011), Cy3-conjugated Goat anti-Mouse IgG (AS008) were purchased from ABclonal Biotech Co., Ltd (Wuhan, China); anti-VEGFA Antibody (ab1316) and anti-p-NF- κ B p65 Antibody (ab32536) were obtained from Abcam (Cambridge, UK); PI3K p85 Mouse mAb (#13666) p-PI3K p85 (#4228), Akt Rabbit mAb (#4691), p-Akt Rabbit mAb (#4060) and p-mTOR Antibody (#2971) were sourced from Cell Signaling Technology (Danvers, MA, USA).

Preparation and Characterization of GaELNs

Fresh garlic (sourced from Pizhou, Jiangsu) was peeled and washed with PBS (pH = 7.2). It was then juiced in a high-speed blender for 2 min at a ratio of 1 g garlic to 10 mL PBS. The resulting juice was filtered through a 300-mesh screen to remove larger particles. The filtrate was then centrifuged at 10,000 g for 30 min at 4 °C and repeatedly centrifuged until no visible precipitate remained. Subsequently, the supernatant was centrifuged at 100,000 g for 2 h at 4 °C. The resulting pellet was resuspended in PBS, then passed through a 0.22 μ m filter (Millipore, MA, USA) under sterile conditions. The final sterile filtrate was collected as GaELNs and stored at –80 °C. Transmission electron microscopy (TEM, Hitachi 7500, Tokyo, Japan) was employed to observe the morphology of GaELNs. Briefly, approximately 10 μ L of GaELNs was placed on a copper grid for 5 min, stained with 2% (w/v) phosphotungstic acid for 3 min, and examined using TEM to observe the exosomal structure.

The NanoSight NS300 instrument (Malvern, Worcestershire, UK) was utilized for nanoparticle tracking analysis (NTA) to determine the size distribution and concentration of GaELNs particles. The protein concentration of GaELNs was assessed using the Bicinchoninic Acid (BCA) Protein Assay Kit (Beyotime Biotechnology, Haimen, China).

Additionally, polyacrylamide gel electrophoresis (PAGE) was employed to analyze the protein composition within the GaELNs.

Metabolomic Analysis of GaELNs

Three batches of GaELNs, prepared at different times, were sent to Majorbio BioPharm Technology Co., Ltd. (Shanghai, China) for metabolomic analysis. In brief, metabolite identification was conducted using an LC-MS/MS system with a Thermo UHPLC-Q Exactive platform. Bioinformatic analyses of the results were performed using the free online Majorbio Cloud Platform (cloud.majorbio.com).

HGF Culture

HGF was obtained from EallBio (Beijing, China). In this study, only in vitro experimental operations were performed on this cell line. There was no direct research on humans, and no identifiable personal information data or biological samples were used. According to Item 1 of Article 32 of the “Measures for Ethical Review of Life Science and Medical Research Involving Human Subjects” in China dated February 18, 2023, which stipulates that “research is conducted using legally obtained public data or data generated through observation without interfering with public behavior”, and Item 2, which states that “research is carried out using anonymized information data”, this study meets the conditions for exemption from ethical review.

Under sterile conditions, the tissue was cultured in DMEM (Gibco, Thermo Fisher Scientific, USA) supplemented with 10% fetal bovine serum (Gibco) and 1% penicillin-streptomycin (Gibco) in a 37 °C incubator with 5% CO₂, with media changes every two days. Gingival fibroblasts from passages three to eight were used for subsequent experiments. HGF from passages three to eight were used for subsequent experiments. In the cellular inflammation treatment model, LPS was added to the culture medium at a concentration of 1 µg/mL and incubated for 24 h, followed by the replacement with fresh medium and the addition of an appropriate concentration of GaELNs for further incubation.

The Experiment for Cellular Uptake of GaELNs

GaELNs were labeled with 3,3'-dioctadecyloxycarbocyanine perchlorate (DIO, Beyotime Biotechnology) for 5 min, followed by centrifugation at 100,000 g for 90 minutes. The supernatant was discarded, and the pellet was resuspended in PBS, repeating this step twice to ensure the removal of unbound dye. DIO-labeled GaELNs were co-cultured with HGF at 37 °C for durations of 1, 6, 12 and 24 h. Subsequently, the cells were fixed with 4% paraformaldehyde (PFA) for 10 minutes, and then stained with DAPI (Beyotime Biotechnology) and 1,1'-dioctadecyl-3,3,3',3'-tetramethylindocarbocyanine perchlorate (DIL, Beyotime Biotechnology) to label the cell nucleus and membrane. Observations were made using a fluorescence microscope.

Cell Viability Assay

The CCK-8 kit (Beyotime Biotechnology) was employed to assess cell viability and the cytotoxic effects of GaELNs at predetermined time points. Briefly, the original culture medium was aspirated from the 96-well plate, and the wells were washed once with PBS. Subsequently, 100 µL of the working solution was added to each well, and the cells were incubated for 1.5 h. The absorbance of each sample was then measured at 450 nm using a microplate reader.

Quantitative Real-Time Polymerase Chain Reaction (qRT-PCR)

For cell samples, 1 mL of TRIzol RNA extraction reagent (Invitrogen) was added to each well of a 6-well plate, and the mixture was carefully pipetted before transferring it to RNA-free EP tubes, followed by lysis on ice for 10 min. For gingival tissue samples, 50–100 mg of tissue was homogenized in 1 mL of TRIzol RNA extraction reagent at 4 °C and subsequently transferred to RNA-free EP tubes. Following the addition of 200 µL of chloroform, the mixture was vortexed for 1 minute and centrifuged at 12,000 g for 10 min at 4 °C. The upper transparent phase was carefully extracted and combined with an equal volume of isopropanol, mixed thoroughly, and incubated on ice for 10 min. Following centrifugation at 12,000 g for 10 min at 4 °C, the supernatant was discarded, and 1 mL of 75% ethanol was added. The mixture was shaken well until visible white mRNA precipitate appeared, followed by a 10-minute incubation on ice.

After centrifugation at 12,000 g for 10 min at 4 °C, the supernatant was removed and allowed to air dry. A small volume of DEPC-treated water was added to resuspend the mRNA, and the concentration was measured using a NanoDrop8000 (Thermo Scientific). Subsequently, the mRNA was normalized in concentration using DEPC-treated water and reverse transcribed into cDNA using the primary script RT kit (Takara, Tokyo, Japan). The TB Green Premix Ex Taq kit (Takara) was utilized for qPCR detection on an ABI QuantStudio 1 fluorescence quantitative PCR instrument (Thermo Scientific). The sequences of the qPCR primers are provided in [Table S1](#) (Shanghai Sangon Biotechnology, Shanghai, China).

ELISA

The ELISA kits were obtained from Solarbio (Beijing, China) and were used in accordance with the manufacturer's instructions. Briefly, the enzyme-linked immunosorbent assay (ELISA) plates were first soaked and then dried, followed by the addition of standard samples and either cell culture supernatants or tissue homogenates, which were incubated at room temperature for 2 h. After the incubation, the liquid was discarded, and the plates were washed four times with wash buffer, then dried. Subsequently, the working solution was added, and the plates were incubated at room temperature with gentle shaking for 1 h. Following this, the plates were washed four additional times with wash buffer, and a chromogenic substrate solution (TMB) was added, allowing color development in the dark at room temperature for 20 min. The reaction was then terminated with a stop solution. Finally, the absorbance values of each well were measured at 450 nm using a microplate reader. A standard curve was constructed based on the concentrations of the standard samples and their corresponding absorbance values, which facilitated the calculation of the target substance concentrations in the test samples.

Detection of Intracellular ROS

The DCFH-DA fluorescent probe (Beyotime) was utilized to detect intracellular ROS. In summary, the procedure was conducted in accordance with the manufacturer's instructions: after treatment, live cell samples were incubated with the DCFH-DA working solution for 30 min, followed by two washes with PBS. Hoechst stain was used to label the cell nuclei, and subsequently, observations were made using a fluorescence microscope.

Western Blot

After the removal of the culture medium from the HGF samples, RIPA buffer containing a protease inhibitor (200 µL for 6-well plates) was added. Cells were thoroughly lysed on ice for 30 min using a cell scraper, and the lysate was then transferred to an EP tube and centrifuged at 12,000 g for 5 min at 4 °C. The BCA Protein Assay Kit was employed to determine the protein concentration in the supernatant. Subsequently, an appropriate volume of PBS and SDS-PAGE loading buffer was added to standardize the protein concentration across the different groups. Using a precast gel, 5 µL of a preset protein marker (Thermo Scientific) was loaded as a molecular weight reference standard, followed by the samples for electrophoresis. Upon completion of the electrophoresis, the proteins in the gel were transferred to a polyvinylidene fluoride (PVDF) membrane (Beyotime), which was then blocked with 5% non-fat dry milk at room temperature for 1 h. Following this, the primary antibody was applied and incubated overnight on a shaker at 4 °C. Tris-buffered saline was utilized to wash the membrane, and a secondary antibody was incubated for 90 min. The ECL Western Blotting Detection Kit (Solarbio) was employed for chemiluminescent detection of the PVDF membrane.

Flow Cytometry

Following the manufacturer's instructions, the processed cells were digested with trypsin to prepare a cell suspension. After centrifugation and discarding the supernatant, the cells were resuspended in a medium containing the fluorescent staining working solution and incubated at 37 °C. The cells were then washed with PBS to remove any unbound dye. The labeled cells were subsequently analyzed using flow cytometry.

Construction of RNA Sequencing Libraries and Sequencing

The processed HGF samples were lysed using TRIzol reagent (Thermo Fisher Scientific) to extract total RNA. The RNA quality was checked by Agilent 2200 and kept at -80 °C. The RNA with RIN (RNA integrity number) > 7.0 is acceptable

for cDNA library construction. The cDNA libraries were constructed for each RNA sample using the VAHTS Universal V6 RNA-seq Library Prep Kit for Illumina (vazyme, Inc.) according to the manufacturer's instructions. Generally, the protocol consists of the following steps: Poly-A containing mRNA was purified from 1 µg total RNA using oligo(dT) magnetic beads and fragmented into 200–600 bp using divalent cations at 85 °C for 6 min. The cleaved RNA fragments were used for first- and second-strand complementary DNA (cDNA) synthesis. dUTP mix was used for second-strand cDNA synthesis, which allows for the removal of the second strand. The cDNA fragments were end repaired, A-tailed and ligated with indexed adapters. The ligated cDNA products were purified and treated with uracil DNA glycosylase to remove the second-strand cDNA. Purified first-strand cDNA was enriched by PCR to create the cDNA libraries. The libraries were quality controlled with Agilent 2200 and sequenced by DNBSEQ-T7 on a 150 bp paired-end run.

Bioinformatics Analysis

Before read mapping, clean reads were obtained from raw reads by removing adaptor sequences and low-quality reads. The clean reads were aligned to Human genome (GRCh38, Ensembl104) using the STAR software. HTseq was used to get gene counts, and the RPKM method was used to determine gene expression levels. The DESeq2 algorithm was applied to filter differentially expressed genes. After significant analysis, P-value and FDR analysis were subjected to the criteria of Fold Change > 2 or < 0.5 and FDR < 0.05 . Gene Ontology (GO) analysis was performed to elucidate the biological implications of differentially expressed genes. GO annotations were downloaded from NCBI, UniProt, and the Gene Ontology database. Fisher's exact test was applied to identify significant GO categories with a P-value < 0.05 . Pathway analysis was used to find significant pathways of differentially expressed genes according to the KEGG database. Fisher's exact test was applied to select significant pathways with a threshold of significance defined by P-value < 0.05 .

Cell Immunofluorescence Staining

The processed HGF samples were fixed with 4% paraformaldehyde for 10 min. Subsequently, 0.1 Triton X-100 (Beyotime) was added and the cells were permeabilized at room temperature for 10 min. After washing, the samples were blocked with 5% BSA (Beyotime) for 1 hour to reduce nonspecific binding. The appropriately diluted primary antibody was then added and incubated overnight at 4 °C for 12 h. The following day, the samples were washed three times with PBS, and fluorescently labeled secondary antibody was added and incubated at room temperature in the dark for 1 h. To stain the cell nuclei, DAPI dye was added and incubated at room temperature for 5 min. After staining, the cells were thoroughly washed. Finally, the samples were observed under a fluorescence microscope, and the desired fluorescence signals were detected using appropriate filters.

Animal Experiment

All animal experiments were conducted in accordance with the ethical policies and procedures approved by the Ethics Committee of Peking University Health Science Center (Approval No.LA2022424). Six-week-old male C57BL/6 mice were purchased from the Animal Department of Peking University Health Science Center (Beijing, China). Mice were randomly assigned to four groups and housed in ventilated animal cabinets under pathogen-free conditions, maintained at 25 °C with a 12 h light-dark cycle, with ad libitum access to food and water. After a three-day acclimatization period, anesthesia was induced using sodium pentobarbital. For the periodontitis and treatment groups, 5–0 silk sutures were placed around the cervical region of the bilateral first molars, while no ligation was performed in the control and GaELNs groups. Subsequently, in the GaELNs group, at days 3, 5, 7, 9 and 11, GaELNs with a concentration of 100 µg/mL were injected into four specific sites (buccal, lingual, mesial, and distal) in the periodontal area. Each site received an injection volume of 10 µL. For the control and periodontitis groups, the same injection method was applied, but with an equal volume of PBS instead. On day 14, the mice were euthanized, and the mandible along with the gingival tissue surrounding the first molars was collected for subsequent experiments.

Micro-CT

After fixation with 4% paraformaldehyde, the mandibles of the mice were placed on the micro-CT scanning platform, and their positions were adjusted to ensure that the scanning area focused on the periodontal tissues and alveolar bone surrounding the first molars. Scanning was performed using a resolution parameter of 10 micrometers. Upon completion of the scan, the image data were exported for quantitative analysis of bone density, bone volume fraction, and other metrics to evaluate changes in the alveolar bone.

Histological Analysis

The mouse mandibles fixed in 4% paraformaldehyde were decalcified using a 10% EDTA solution for two weeks, with daily changes of the EDTA solution. Subsequently, the tissues were embedded in paraffin and sectioned into 7-micrometer slices. For hematoxylin and eosin (H&E) staining, the slices were deparaffinized, rehydrated, stained with hematoxylin for 10 min, rinsed with tap water, differentiated with hydrochloric acid-ethanol, and blued with ammonia water, followed by eosin staining for 1 min, dehydration, clearing, and mounting. For TRAP staining, the slices were deparaffinized and incubated with TRAP working solution according to the kit instructions for approximately 1 hour, with red staining indicating osteoclast activity, followed by dehydration and mounting. For immunofluorescence staining, the slices were deparaffinized and rehydrated, subjected to antigen retrieval using citrate buffer at 95°C for 20 min, cooled, and then incubated with blocking solution for 1 h. Subsequently, the primary antibody was added and incubated overnight at 4 °C. After washing, the secondary antibody was applied and incubated in the dark for 1 h, followed by DAPI staining for nuclear labeling. Finally, the slices were mounted using an anti-fade mounting medium.

Cell Immunofluorescence and Mitochondrial Morphology Co-Staining

The processed cells were first incubated with Mito-Tracker working solution for 30 min, followed by gentle washing three times with PBS buffer. Subsequently, the cells were fixed at room temperature with 4% paraformaldehyde for 10 min. After rinsing with PBS, 0.1% Triton X-100 was added to permeabilize the cells for 10 min, and then the cells were blocked with 5% BSA at room temperature for 1 h. The primary antibody was then added and incubated overnight at 4 °C. After washing with PBS, the cells were incubated with a fluorescence-labeled secondary antibody for 1 h at room temperature. Finally, the nuclei were stained with Hoechst for 5 min, and images were captured under a fluorescence microscope.

Mitochondrial ROS Detection

The treated HGF were incubated with Mito-SOX Reagent working solution for 10 min to label the ROS within the mitochondria. Subsequently, the cells were washed three times with PBS to remove any unbound dye. The cells were then fixed with 4% paraformaldehyde for 10 minutes, followed by another wash with PBS. Next, the cells were permeabilized with 0.1% Triton X-100 for 10 min, and then incubated with a blocking solution at room temperature for 1 h, followed by three washes with PBS. Finally, the cells were stained with Hoechst for 5 min, and the images were captured using a fluorescence microscope.

Mitochondrial Membrane Potential Detection

The processed HGF cells were incubated with TMRM working solution for 30 min, followed by fixation with 4% paraformaldehyde for 10 min. After washing with PBS, the cells were stained with Hoechst for 5 min. Fluorescent microscopy was then employed to observe and capture images.

Quantification of Mitochondrial DNA in the Cytoplasm

The extraction of cytoplasmic DNA was performed using the QIAamp DNA Mini Kit (Qiagen, Germany) according to the manufacturer's instructions. The processed HGF were resuspended in an appropriate volume of cell lysis buffer and incubated at room temperature for 5 min before transferring to the QIAamp column. Centrifugation was carried out, followed by the addition of wash buffer to remove impurities; a subsequent centrifugation was performed, and the DNA

was eluted using AE buffer. The extracted cytoplasmic DNA was quantified for concentration and purity using Nanodrop. Subsequently, primers specific to the mitochondrial gene (ND1) were utilized to assess the levels of mtDNA in HGF, with nuclear 18S rRNA serving as a loading control.

Statistical Analysis

Statistical analyses were conducted using GraphPad Prism (version 9.0.0). Data are expressed as mean \pm standard deviation (SD). Unpaired two-tailed Student's *t*-tests were employed for comparisons between two groups. For experiments involving comparisons among three or more groups, ordinary one-way analysis of variance (ANOVA) was applied, followed by post hoc tests for multiple comparisons. In multi-factor experiments with three or more groups, two-way ANOVA was utilized, also followed by post hoc tests for multiple comparisons. A *p*-value less than 0.05 was considered statistically significant.

Results

Characterization and Functional Screening of GaELNs

We developed a simplified method for isolating exosomes from fresh garlic (Figure 1A). Following peeling and rinsing, fresh garlic was juiced and filtered to obtain the filtrate. Large particles were removed by repeated high-speed centrifugation, while exosome-like nanovesicles were isolated via ultracentrifugation. Finally, a 0.22 μm sterile filter was employed to purify the exosome-like nanovesicles and eliminate bacterial contaminants. This protocol did not require additional reagents beyond PBS and yielded approximately 300–400 mg of GaELNs per 100 g of garlic, comparable to yields obtained by other methods.¹⁹ Furthermore, the Pearson correlation coefficients between the three independently prepared GaELNs batches was consistently above 0.9, which further confirms the stability and reliability of our GaELN isolation method³⁰ (Figure S1). Nanoparticle Tracking Analysis (NTA) indicated a particle concentration of 1×10^{11} particles/mL, with an average particle diameter of 52 nm, ranging between 30–200 nm (Figure 1B). Transmission Electron Microscopy (TEM) revealed that GaELNs exhibit a discoidal morphology with central concavities (Figure 1C). SDS-PAGE analysis demonstrated that the protein content of GaELNs ranged between 20 kDa and 60 kDa (Figure 1D). GaELNs-Dio were readily internalized by gingival fibroblasts after 1 hour of co-culture, with uptake significantly increasing over time (Figure 1E and F), confirming the successful isolation of GaELNs and their excellent cellular compatibility. To further investigate the contents and potential biological effects of GaELNs, high-resolution mass spectrometry was employed, identifying a total of 847 metabolites, including amino acids and derivatives (17.89%), lipids (19.3%), terpenes (7.49%), flavonoids (2.57%) and coumarin derivatives (2.57%), among various other biologically active substances (Figure 1G). Representative compounds are listed in Table S2; according to current research, their functions are closely associated with metabolic regulation, antioxidant activity, anti-inflammatory properties, anti-tumor effects, neuroprotection, immune modulation and the promotion of cell proliferation.^{31–34} Additionally, KEGG enrichment analysis of the metabolite profile indicated associations with tumor metabolism, mTOR signaling pathways and NF- κ B signaling pathways (Figure 1H), strongly suggesting a relationship with metabolic reprogramming.

GaELNs Promote Cell Proliferation and Migration

The appropriate concentration of GaELNs was screened through the CCK-8 assay (Figure 2A), which indicated that co-culturing with cells for 48 h at 100 $\mu\text{g}/\text{mL}$ significantly enhanced cell viability, whereas concentrations of 200 $\mu\text{g}/\text{mL}$ and above markedly inhibited cell viability. CFDA-SE fluorescent staining demonstrated cellular proliferation, revealing that after normal culture for 48 h with GaELNs, there was a pronounced increase in cell proliferation, exhibiting a concentration-dependent effect within the 100 $\mu\text{g}/\text{mL}$ range (Figure 2B). The results of the scratch assay indicated that the healing of cell scratches was significantly accelerated after the addition of GaELNs for both 24 and 48 h (Figure 2C), with quantitative analysis showing that GaELNs at 100 $\mu\text{g}/\text{mL}$ notably enhanced cell migratory capacity after 24 h of co-culture, with this effect further amplified following 48 h of culture (Figure 2D). Additionally, the immunofluorescence results for VEGF indicated weaker fluorescence intensity in the control group, reflecting low expression levels of VEGF

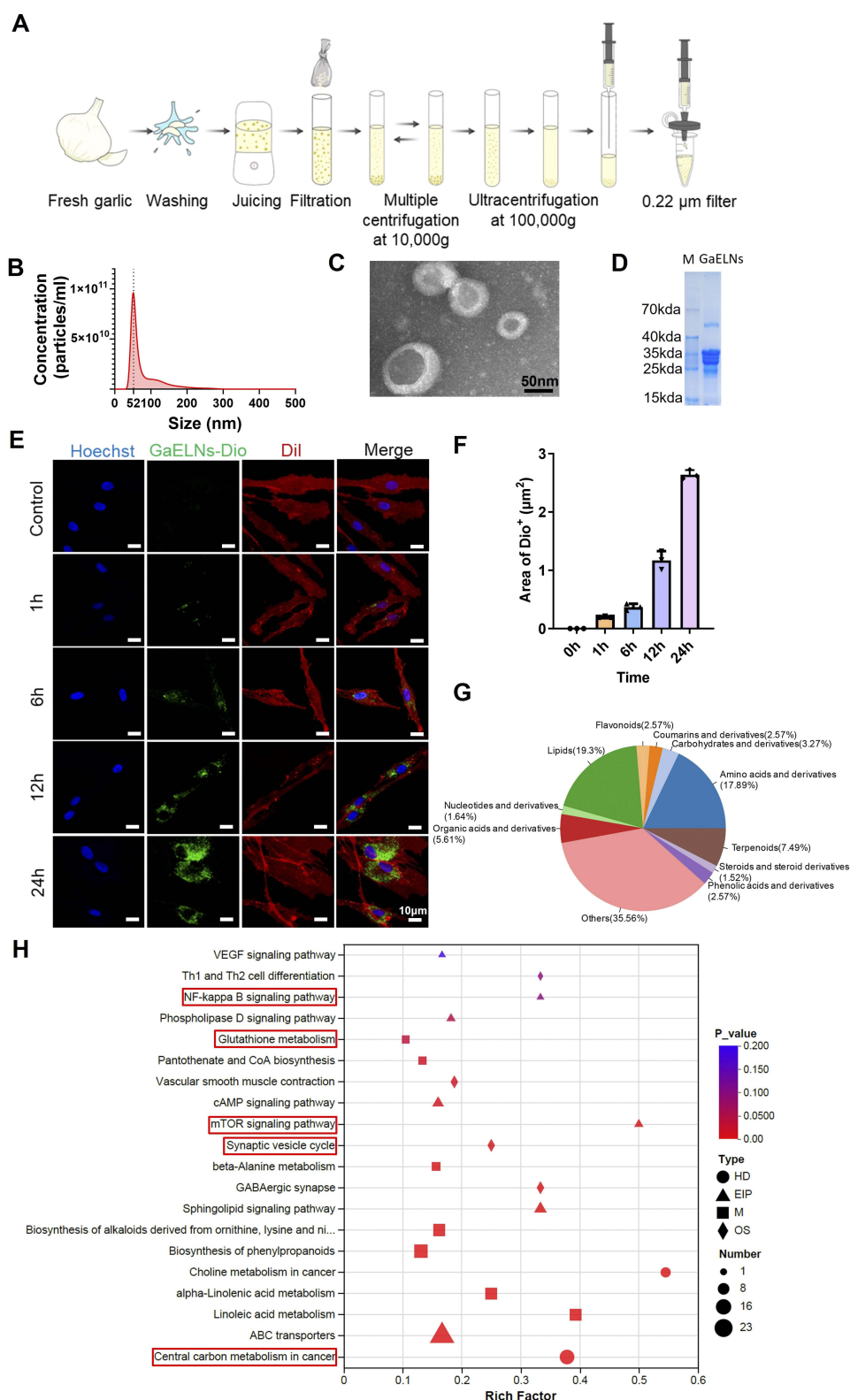


Figure 1 Characterization and Metabolomic Analysis of GaELNs. **(A)** Protocol for GaELNs extraction process. **(B)** NTA analysis showing particle size distribution of GaELNs. **(C)** TEM imaging depicting GaELNs morphology. Scale bar = 50 nm. **(D)** SDS-PAGE analysis illustrating the protein distribution in GaELNs. (M) maker. **(E)** Fluorescence microscopy images displaying the localization of GaELNs in HGF cells at 1, 6, 12 and 24 h. Scale bar = 10 μm. **(F)** Semi-quantitative analysis of the green fluorescent area representing GaELNs-Dio in cells (n=3). **(G)** Pie chart illustrating classification of metabolites contained within GaELNs (n=3). **(H)** KEGG pathway enrichment analysis of GaELNs' metabolite set. The red boxes highlight signaling pathways associated with inflammation, metabolism, tumor progression and neurological functions.

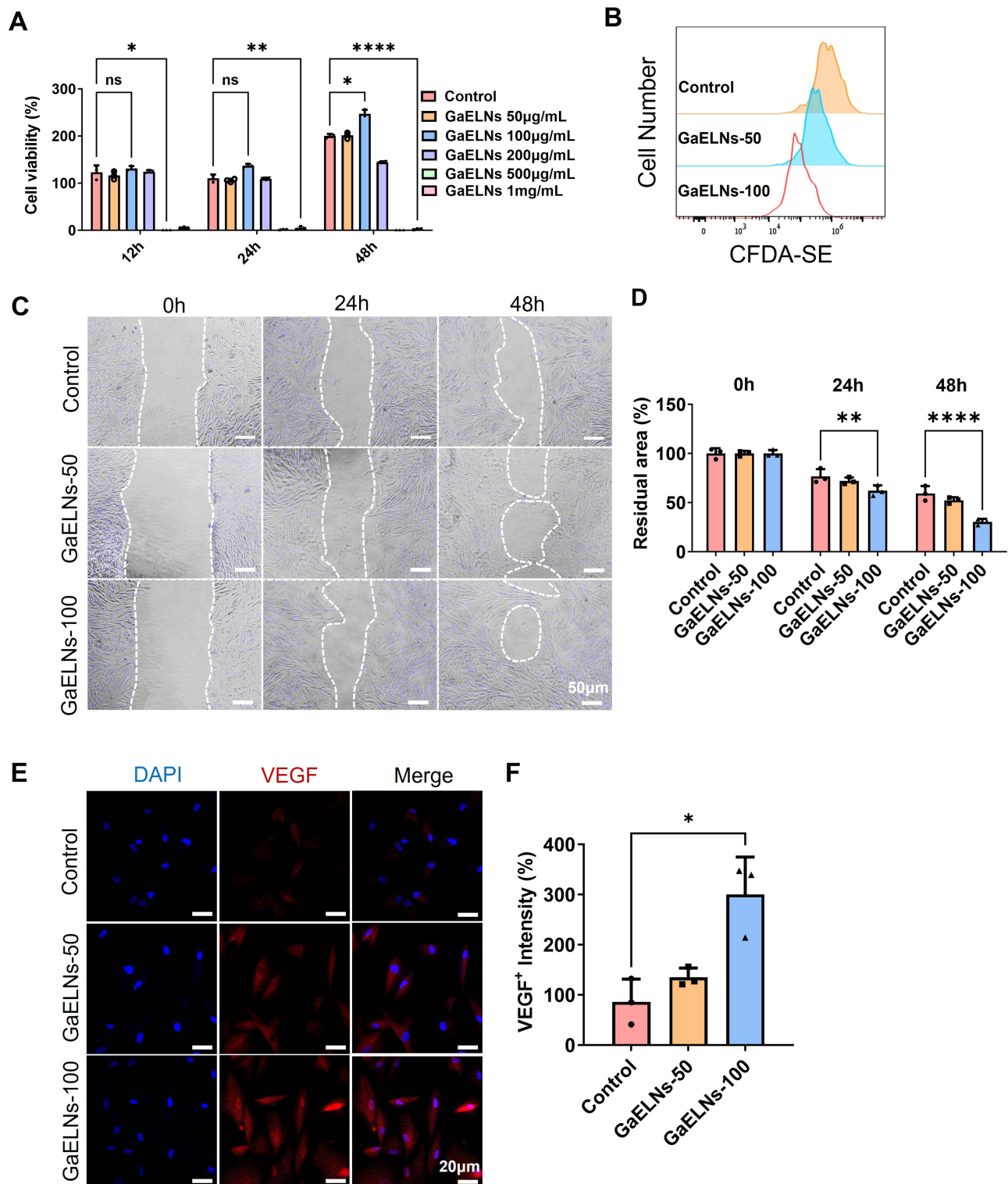


Figure 2 GaELNs Promote Proliferation, Migration and VEGF Expression in HGF. (A). CCK-8 assessing the effect of GaELNs on cell viability across concentrations ranging from 50 µg/mL to 1 mg/mL, with incubation times of 12, 24 and 48 h (n=3). (B). Flow cytometry analysis of GaELNs' effect on proliferation in CFDA-SE labeled HGF. GaELNs-50: GaELNs 50 µg/mL. GaELNs-100: GaELNs 100 µg/mL. (C and D). Scratch assay evaluating the impact of GaELNs on HGF migration capacity and semi-quantitative analysis of migration distance (n=3). (E). Immunofluorescence analysis of VEGF expression in HGF influenced by GaELNs. Scale bar = 20 µm. (F). Semi-quantitative analysis of VEGF fluorescence intensity (n=3). All data are expressed as mean ± SD, *p < 0.05, **p < 0.01, ****p < 0.0001.

in normal cells; both 50 $\mu\text{g/mL}$ and 100 $\mu\text{g/mL}$ GaELNs promoted VEGF expression in a concentration-dependent manner (Figure 2E and F). These findings suggest that 100 $\mu\text{g/mL}$ GaELNs exert a highly positive influence on cells. In subsequent experiments, unless otherwise stated, 100 $\mu\text{g/mL}$ GaELNs were utilized.

GaELNs Attenuate LPS-Induced Cellular Inflammatory Responses and Oxidative Stress

qPCR and ELISA assays were employed to investigate the transcription and expression of inflammation-associated factors modulated by GaELNs in LPS-induced cells. As shown in Figure 3A–D, the mRNA level of pro-inflammatory factors CXCL-12, CXCL-5, CXCL-6 and IL-12 significantly increased following LPS stimulation, while a substantial reduction in mRNA levels was observed in the LPS + GaELNs group. ELISA results further demonstrated that the addition of GaELNs effectively reduced the secretion of these pro-inflammatory cytokines following LPS stimulation. (Figure 3E–H), demonstrating the potent anti-inflammatory properties of GaELNs. Subsequently, we examined the oxidative stress status within the cells. The DCFH-DA fluorescent probe was used to monitor changes in intracellular ROS levels. ROS accumulation remained low under normal conditions or upon treatment with GaELNs alone; however, ROS levels markedly increased following LPS treatment, while the LPS + GaELNs group showed a significant reduction in ROS (Figure 3I). Additionally, qPCR results revealed that the transcription levels of oxidative stress-protective factors CAT, GSR, HO-1 and NQO1 were notably decreased in the LPS group, with this effect partially reversed in the LPS + GaELNs group (Figure 3J–M). Western blot (WB) analysis corroborated the qPCR findings, showing that the expression of HO-1, Nrf2 and NQO1 was significantly downregulated in the LPS group, while significantly upregulated in the LPS + GaELNs group (Figure 3N–Q). These results demonstrate that GaELNs exhibit pronounced anti-inflammatory and antioxidant effects by suppressing pro-inflammatory factor expression and reducing ROS levels. Through upregulation of antioxidant genes and proteins, GaELNs contribute to mitigating LPS-induced cellular inflammation and oxidative stress.

GaELNs Alleviate Bone Resorption and Gingival Inflammation in Mice with Periodontitis

A classical model of experimental periodontitis was established by ligating the bilateral mandibular first molars of mice for two weeks, during which freshly prepared GaELNs or PBS were administered via local injection around the first molars a total of five times. None of the groups caused visceral lesions or toxicity in the mice (Figure S2). Micro-CT 3D reconstruction of the mandibles revealed that alveolar bone height in mice receiving GaELNs alone was comparable to the control group, whereas the Perio group exhibited significant bone height reduction and notable furcation defects; in contrast, the Perio + GaELNs group demonstrated marked restoration of alveolar bone height with partial bone fill in the furcation region (Figure 4A). Quantitative analysis of the cemento-enamel junction-to-alveolar bone crest (CEJ-ABC) distance confirmed that this metric was significantly increased in the Perio group compared to the control and GaELNs groups, while it was significantly reduced in the Perio + GaELNs group relative to the Perio group (Figure 4B). Additionally, bone volume fraction (BV/TV) and bone mineral density (BMD) were significantly reduced in the Perio group compared to control and GaELNs groups, whereas marked improvements were observed in the Perio + GaELNs group (Figure 4C and D). Histological analysis further examined periodontal changes across the four groups. H&E staining indicated a notable increase in periodontal ligament width in the Perio group, while the Perio + GaELNs group showed partial reversal of periodontal defects and reduction in alveolar bone resorption (Figure 4E). Analysis of the distance between the furcation roof and alveolar crest demonstrated a significant reduction in the Perio + GaELNs group compared to the Perio group (Figure 4F). Moreover, tartrate-resistant acid phosphatase (TRAP) staining revealed a significant increase in TRAP⁺ osteoclasts in the Perio group, while the Perio + GaELNs group exhibited reduced TRAP⁺ cell numbers (Figure 4G and H), suggesting that GaELNs may inhibit osteoclastogenesis and thereby mitigate periodontitis-associated bone resorption. Additionally, we assessed local gingival inflammatory cytokines; both qPCR and ELISA results showed significantly lower expressions of TNF- α , CXCL-12, CXCL-5 and IL-12 in the Perio + GaELNs group compared to the Perio group (Figure 4I–P). In summary, local administration of GaELNs significantly attenuates inflammatory responses and bone loss associated with periodontitis.

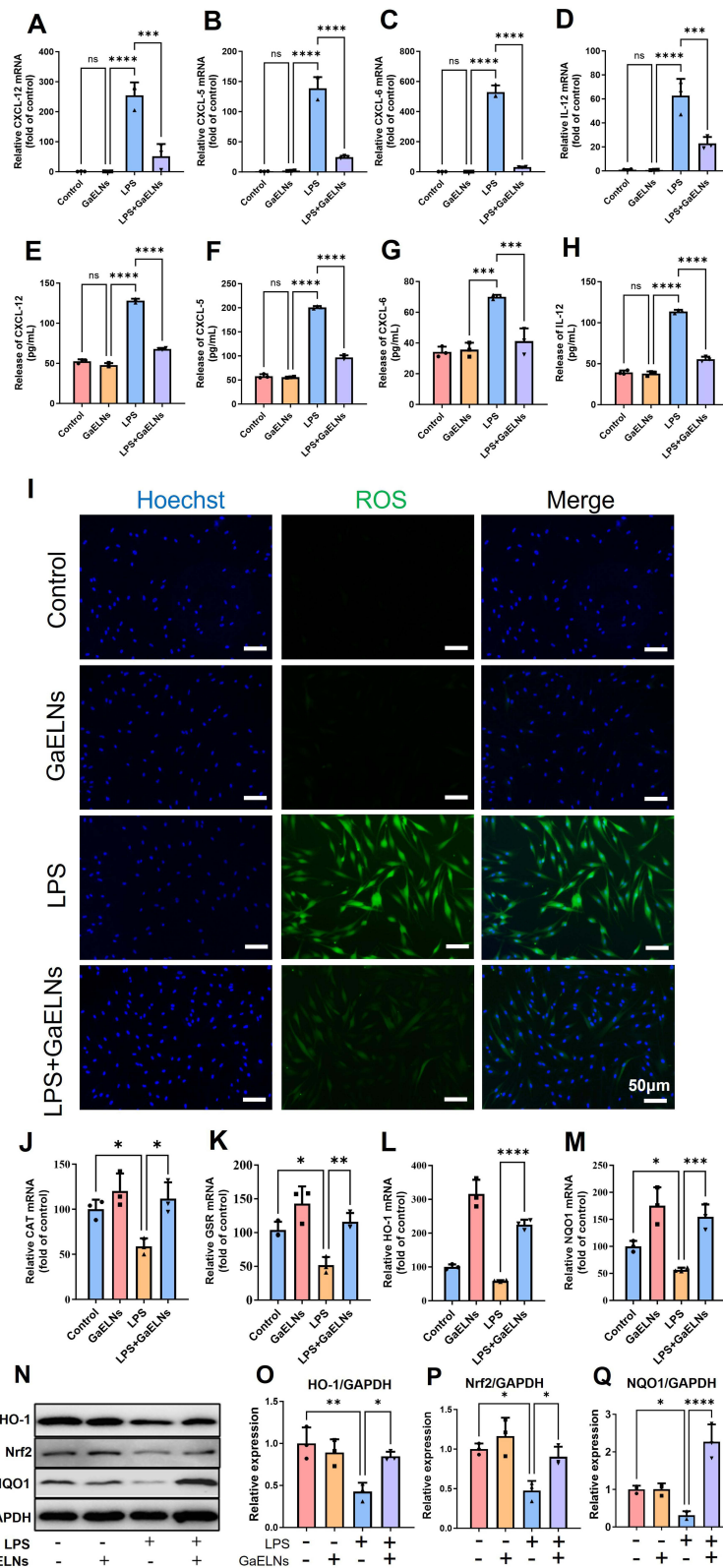


Figure 3 Inhibitory Effects of GaELNs on LPS-Induced Inflammation and Oxidative Stress in HGF. **(A–D)** qPCR analysis of mRNA levels of pro-inflammatory factors CXCL-12, CXCL-5, CXCL-6 and IL-12 under different treatments in HGF (n=3). **(E–H)** ELISA quantification of extracellular secretion levels of CXCL-12, CXCL-5, CXCL-6 and IL-12 in HGF (n=3). **(I)** DCFH-DA fluorescent probe assay indicating intracellular ROS levels in HGF under different treatments. Scale bar = 50 μm. **(J–M)** qPCR analysis of mRNA levels of oxidative stress-related factors CAT, GSR, HO-1 and NQO1 in HGF cells under different treatments (n=3). **(N)** WB analysis of HO-1, Nrf2, NQO1 and GAPDH expression levels in whole cell lysates. **(O–Q)** Relative expression levels of HO-1/GAPDH, Nrf2/GAPDH and NQO1/GAPDH determined from band intensities. All data are expressed as mean ± SD, *p < 0.05, **p < 0.01, ***p < 0.001, ****p < 0.0001.

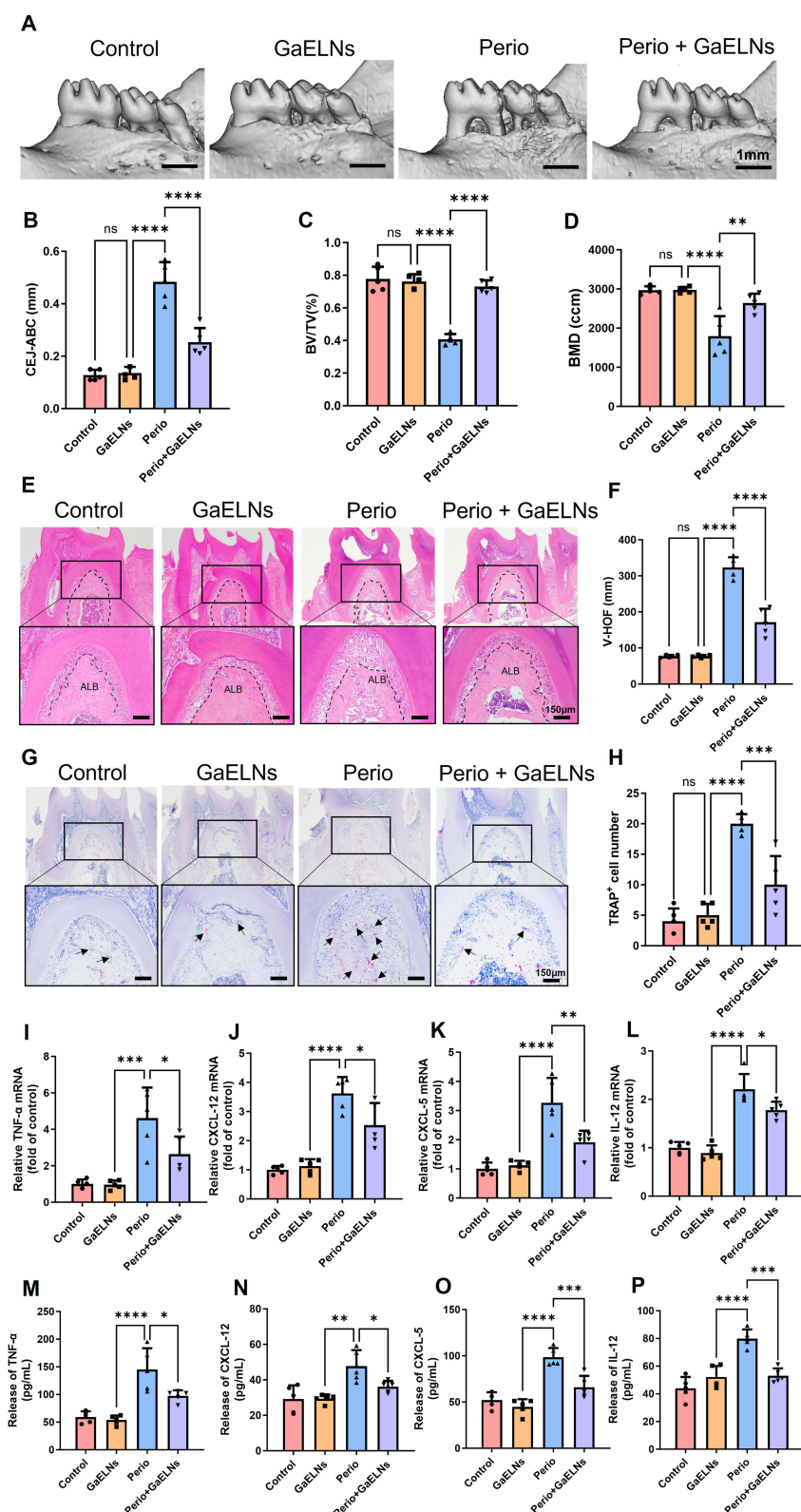


Figure 4 Therapeutic Effects of GaELNs on Periodontitis in Mice (n=5). **(A)** 3D reconstructed images of mouse mandibles using Micro-CT. Perio: periodontitis. Scale bar = 1 mm. **(B–D)** Quantification of the distance from the cemento-enamel junction (CEJ) to the alveolar bone crest (ABC) (ABC-CEJ), bone volume fraction (BV/TV) and bone mineral density (BMD) (n=5). **(E)** Representative H&E-stained sections of the first molar region in mouse mandibles. ALB, alveolar bone. Scale bar = 150 μm **(F)** Quantification of the distance between the furcation roof and the alveolar bone crest (vertical height of furcation [V-HOF]) (n=5). **(G and H)** TRAP staining showing osteoclast numbers in alveolar bone across groups, with semi-quantitative analysis (n=5). Scale bar = 150 μm. **(I–L)** qPCR analysis of mRNA levels of pro-inflammatory factors TNF-α, CXCL-12, CXCL-5 and IL-12 in gingival tissue. **(M–P)** ELISA analysis of pro-inflammatory factor levels for TNF-α, CXCL-12, CXCL-5 and IL-12 in gingival tissue. All data are expressed as mean ± SD, *p < 0.05, **p < 0.01, ***p < 0.001, ****p < 0.0001.

Omics Analysis Revealed That GaELNs Alleviate Inflammatory Responses Through Mechanisms of Metabolic Reprogramming

To elucidate the molecular mechanisms underlying the biological effects of GaELNs, we performed transcriptome sequencing on the control, GaELNs, LPS and LPS+GaELNs groups, and conducted an integrated analysis with the metabolomics data of GaELNs. Compared to the LPS group, the LPS+GaELNs group exhibited 492 downregulated genes and 625 upregulated genes (Figure 5A), while the LPS group versus the control group showed 3,554 upregulated and 3,025 downregulated genes (Figure S3A), and the GaELNs group had 2,257 downregulated and 86 upregulated genes (Figure S3B). Notably, pro-inflammatory genes, including MMP3, CXCL6, IL12A and CXCL8, were significantly upregulated by LPS stimulation but markedly downregulated in the LPS+GaELNs group. Additionally, genes involved in regulating cellular metabolism, promoting proliferation and inhibiting inflammation and oxidative stress, such as FTH1P, PDK2, TIMP1 and PHGDH, were significantly upregulated with GaELNs treatment (Figure S3C). To identify potential target genes of GaELNs, we intersected the LPS-downregulated gene set, the GaELNs-upregulated gene set and the LPS+GaELNs-upregulated gene set, identifying 12 overlapping genes (Figure 5B), among which PHGDH showed the most pronounced expression changes across

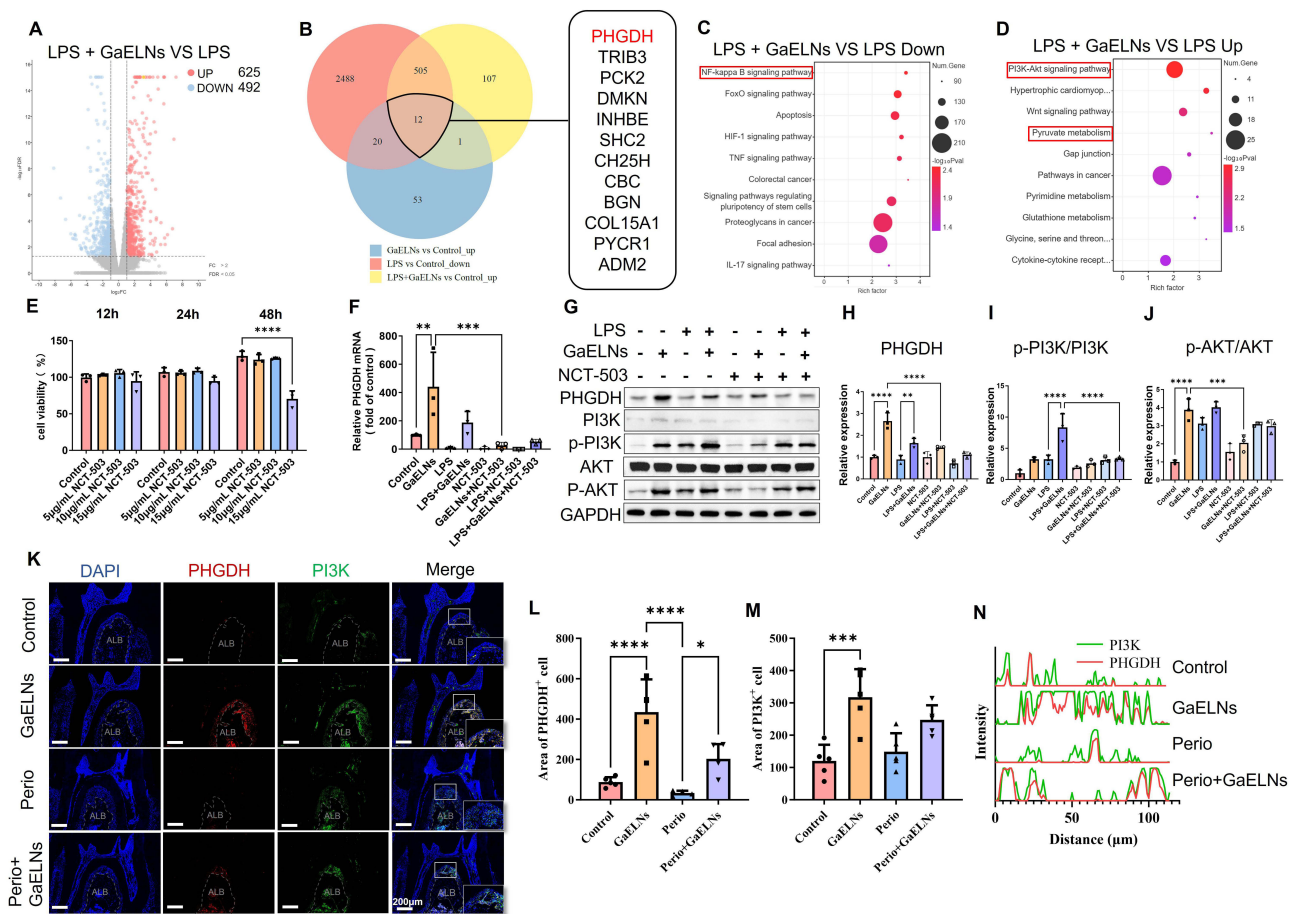


Figure 5 GaELNs Treat Periodontitis by Activating the PHGDH/PI3K/AKT Pathway. (A) Volcano plot showing differentially expressed genes between the LPS + GaELNs and LPS groups. (B) Venn diagram illustrating the overlap among gene sets “GaELNs vs Control upregulated”, “LPS vs Control downregulated” and “LPS + GaELNs vs Control upregulated” with 12 genes common to all three groups. (C) KEGG pathway analysis of genes upregulated in the LPS + GaELNs group compared to the Control group. The red boxes highlight signaling pathways associated with inflammation and metabolism. Up: upregulated. (D) KEGG pathway analysis of genes downregulated in the LPS + GaELNs group compared to the Control group. (E) CCK-8 showing cell viability changes over time with different concentrations of NCT-503 co-cultured with HGF. (F) qPCR analysis of PHGDH mRNA levels in HGF under different treatment conditions. (G) WB analysis of PHGDH, PI3K, p-PI3K, AKT, p-AKT and GAPDH expression levels in whole cell lysates. (H–J). Relative protein expression levels of PHGDH/PI3K, p-PI3K/PI3K and p-AKT/AKT based on band intensities (n=3). (K). Immunofluorescence staining for PHGDH and PI3K in tissue sections of the first molar of the mouse mandible. Gray solid lines were used for fluorescence colocalization analysis of PHGDH and PI3K. Scale bar = 200 μm. (L and M). Semi-quantitative analysis of red fluorescence for PHGDH and green fluorescence for PI3K (n=5). (N). Colocalization analysis of PHGDH red fluorescence and PI3K green fluorescence along the grayscale line. All data are expressed as mean ± SD, *p < 0.05, **p < 0.01, ***p < 0.001, ****p < 0.0001.

groups. PHGDH, a key enzyme in the serine biosynthesis pathway, catalyzes the conversion of the glycolytic intermediate 3-phosphoglycerate to 3-phosphohydroxypyruvate, thereby supplying non-essential amino acids like serine for cellular energy metabolism.^{35,36} PHGDH also enhances antioxidant production via the serine synthesis pathway, helping to maintain intracellular redox balance, reduce mitochondrial oxidative stress and preserve mitochondrial function.^{37,38} Furthermore, studies have shown that PHGDH itself can directly regulate cellular metabolism, proliferation and immune inflammation,^{39,40} enhancing the PI3K/AKT signaling pathway to promote cell proliferation,^{41,42} support cellular growth and ameliorate abnormal inflammatory states. Moreover, KEGG pathway analysis revealed that in comparison to the LPS group, the LPS + GaELNs group demonstrated a significant downregulation in pro-inflammatory signaling pathways, including the NF- κ B signaling pathway, Apoptosis, TNF signaling pathway and IL-17 signaling pathway, while showing significant upregulation in the PI3K/AKT signaling pathway and metabolism-related pathways (Figure 5C and D), which aligns with the metabolomics findings of GaELNs. The PI3K/AKT pathway is closely associated with cell survival, proliferation, migration and metabolic reprogramming. Its notable upregulation may indicate cellular entry into a repair and regeneration state following inflammation reduction and it promotes cell survival and improved metabolism through downstream effectors, such as mTOR and Nrf2.^{43–45} GSEA further illustrated gene expression changes within specific pathways, showing that, relative to the LPS group, the pyruvate metabolism pathway, amino acid biosynthesis and mitochondrial autophagy-related genes were significantly upregulated following GaELNs treatment, while the NF- κ B signaling pathway was significantly downregulated (Figure S3D). Collectively, sequencing results indicate that the biological effects of GaELNs are closely associated with metabolic reprogramming, with PHGDH and the PI3K/AKT signaling pathway potentially playing critical roles in these effects.

GaNELs Promote the Expression of PHGDH, Which Shows a Significant Positive Correlation with the PI3K/AKT Pathway

To further investigate the relationship between GaELNs and the PHGDH/PI3K/AKT signaling pathway, including downstream effectors, we utilized NCT-503 to inhibit PHGDH expression. At a concentration of 15 μ g/mL, NCT-503 exhibited clear cytotoxicity at 48 h, while concentrations of 10 μ g/mL and below showed no cytotoxic effects (Figure 5E); therefore, 10 μ g/mL NCT-503 was selected for subsequent experiments. Under normal conditions, GaELNs significantly increased PHGDH mRNA level, while the addition of NCT-503 effectively inhibited PHGDH mRNA level (Figure 5F). WB analysis showed that the band intensity for PHGDH was approximately 2.5 times higher in the GaELNs group compared to the control, with no significant change observed in the LPS group. Upon NCT-503 treatment, PHGDH expression was notably suppressed. Additionally, we examined the levels of activated and phosphorylated PI3K and Akt. Interestingly, both GaELNs and LPS increased phosphorylated PI3K and Akt expression, with the highest expression observed in the LPS + GaELNs group, consistent with multi-omics results. The addition of NCT-503 reduced GaELNs-induced expression significantly, while the LPS-induced expression remained unaffected. This suggests that phosphorylated PI3K and AKT expression is closely linked to PHGDH (Figure 5G–J). Immunofluorescence results from mandibular bone sections of mice were consistent with WB findings, showing low expression of PHGDH and PI3K in periodontal tissues of the control group, while expression was markedly elevated in the GaELNs and Perio + GaELNs groups, with only PI3K expression elevated in the Perio group (Figure 5K–M). Co-expression analysis indicated weak co-expression of PHGDH and PI3K in the control and Perio groups, but strong co-expression in the GaELNs and Perio + GaELNs groups (Figure 5N). Similar results were also observed in the mRNA levels of the gingival tissues of mice. After local injection of GaELNs, the expressions of PHGDH, PIK3CA, and AKT1 were upregulated (Figure S4A–S4C). These findings indicate that GaELNs likely exert their biological effects by elevating PHGDH expression, thereby activating the PI3K/AKT pathway.

GaELNs Promote Cell Proliferation by Enhancing mTOR and VEGF Expression via PHGDH/PI3K/AKT

The PI3K/AKT signaling pathway is capable of activating various downstream signaling molecules to execute distinct functions. mTOR is a classical downstream effector, and following the addition of GaELNs, the expression ratio of p-mTOR was significantly elevated. In contrast, when NCT-503 was administered, the expression ratio of p-mTOR showed no significant difference compared to the control and LPS groups, indicating that GaELNs upregulated the

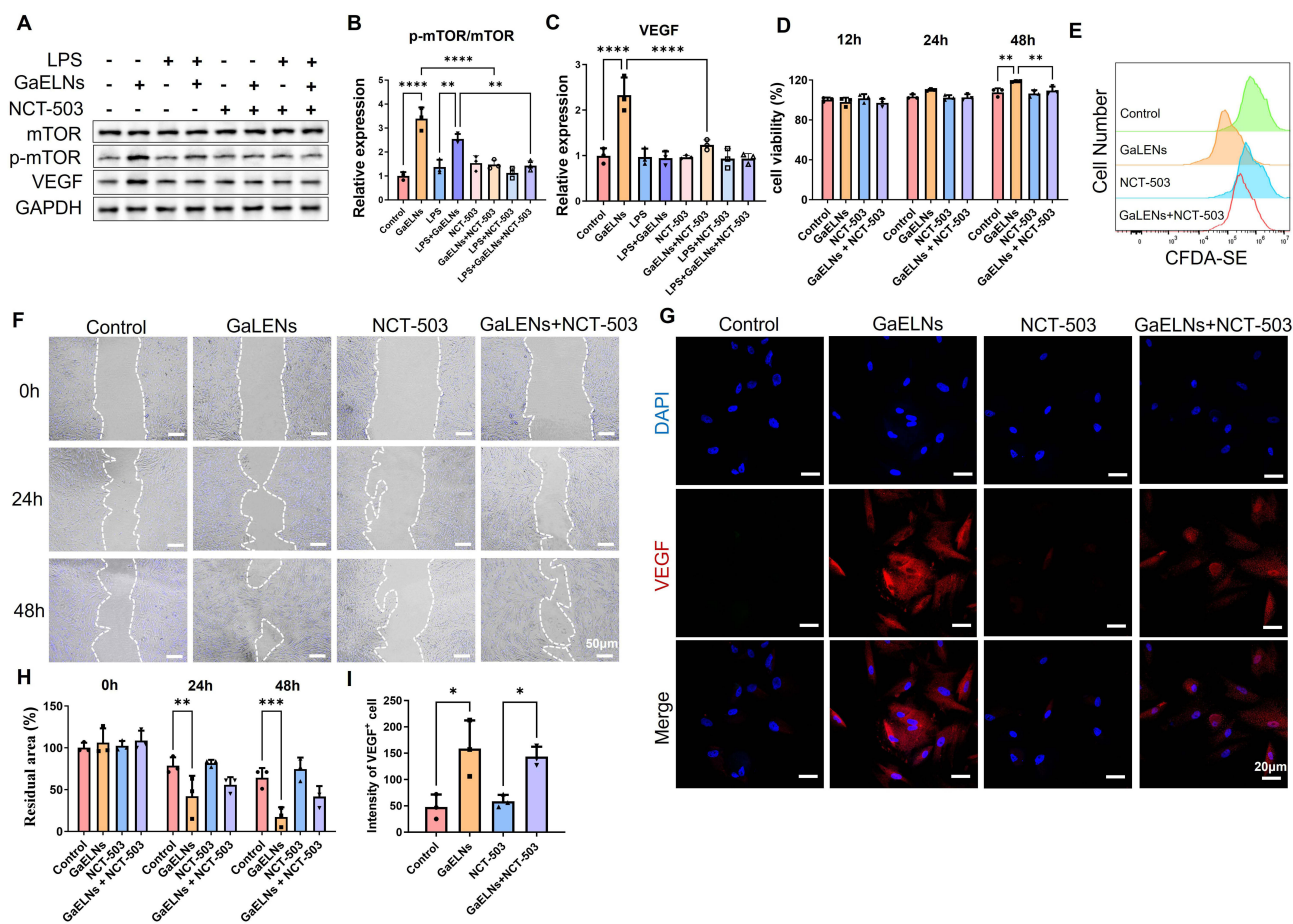


Figure 6 GaELNs Promote Cell Proliferation and Migration by Upregulating mTOR and VEGF Expression via the PHGDH/PI3K/AKT Pathway. **(A)**, WB analysis of mTOR, p-mTOR, VEGF and GAPDH expression levels in whole cell lysates. **(B and C)**, Relative protein expression levels of p-mTOR/mTOR and VEGF/GAPDH based on band intensities (n=3). **(D)**, CCK-8 assay showing changes in HGF cell viability following the addition of GaELNs and NCT-503. **(E)**, Flow cytometry analysis of GaELNs and NCT-503 effects on the proliferation of CFDA-SE-labeled HGF. **(F)**, Scratch assay evaluating the impact of GaELNs and NCT-503 on HGF migration. Scale bar = 50 μ m. **(G)**, Immunofluorescence analysis of VEGF expression in HGF following treatment with GaELNs and NCT-503. Scale bar = 20 μ m. **(H)**, Semi-quantitative analysis of cell migration distance (n=3). **(I)**, Semi-quantitative analysis of VEGF fluorescence intensity (n=3). All data are expressed as mean \pm SD, *p < 0.05, **p < 0.01, ***p < 0.001, ****p < 0.0001.

activity of the mTOR pathway through PHGDH/PI3K/AKT. Additionally, the expression trend of vascular endothelial growth factor (VEGF) was consistent with the changes in p-mTOR, further supporting the interrelationship between the two in the process of cell proliferation. (Figure 6A–C). Concurrently, results from the CCK-8 assay and CFDA-SE fluorescence staining indicate that the addition of NCT-503 suppresses the increase in cell viability and proliferation capabilities mediated by GaELNs (Figure 6D and E). Furthermore, cell scratch assays and subsequent semi-quantitative analyses indicated a slight decrease in cell migration capacity in the GaELNs + NCT-503 group compared to the GaELNs group at both 24 and 48 h (Figure 6F and H). Immunofluorescence results reveal a relative decrease in VEGF expression in the GaELNs+NCT-503 group compared to the GaELNs group (Figure 6G and I). Collectively, these results indicate that the effect of GaELNs in promoting cell proliferation is closely associated with PHGDH, potentially involving the activation of the PI3K/AKT pathway and its downstream signaling molecules, mTOR and VEGF.

GaELNs Reduce Inflammation and Oxidative Stress and Improve Mitochondrial Function via the PHGDH/PI3K/AKT Pathway by Downregulating NF- κ B and Upregulating Nrf2

NF- κ B and Nrf2 are also considered downstream signaling molecules of the PI3K/AKT pathway, with NF- κ B being a classical inflammatory signaling pathway and Nrf2 closely associated with the alleviation of oxidative stress and enhancement of mitochondrial function. WB results indicated that LPS significantly increased the expression ratio of

p-p65 and decreased Nrf2 expression. In contrast, the addition of GaELNs significantly increased Nrf2 expression and notably reduced the elevated expression of p-p65 induced by LPS. The effects of GaELNs were significantly diminished upon the addition of NCT-503. In addition, after local injection of GaELNs, the mRNA level of Nfe2l2 in the gingival tissues of mice was also significantly increased, while the level of RelA was significantly decreased. Immunofluorescence staining of the periodontal tissues demonstrated that the expression of Nrf2 was restored and the expression of p65 was reduced after the injection of GaELNs (Figure S4D-S4G). These results further demonstrate the close correlation with the PHGDH/PI3K/AKT pathway (Figure 7A–C). In addition, intracellular ROS levels showed that, compared to the GaELNs +LPS group, the GaELNs+LPS+NCT-503 group had relatively higher intracellular ROS levels (Figure 7D), indicating that PHGDH plays a critical role in this context.

Intracellular oxidative stress significantly impacts mitochondrial function. To further elucidate the effects of GaELNs and PHGDH on mitochondrial function, we performed co-staining with PHGDH immunofluorescence and Mito-Tractor. In the control group, mitochondria in normal cells exhibited a reticular or elongated morphology; however, following LPS stimulation, the normal mitochondrial structure was lost, presenting instead as punctate and more diffusely distributed, with no apparent PHGDH fluorescence signal observed in either group. In contrast, the GaELNs+LPS group showed a marked increase in normal mitochondrial morphology, along with a significant upregulation of PHGDH expression. Upon addition of NCT-503, PHGDH expression was reduced in the LPS + GaELNs + NCT-503 group and the prevalence of abnormal mitochondrial morphology increased (Figure 7E). We further assessed mitochondrial superoxide levels and membrane potential changes. As shown in fluorescence staining and flow cytometry results (Figure 7F–I), LPS markedly increased mitochondrial superoxide and decreased mitochondrial membrane potential, while GaELNs administration significantly reduced mitochondrial superoxide and partially improved membrane potential. When NCT-503 was used, the beneficial effects of GaELNs were markedly suppressed. Additionally, LPS stimulation induced substantial mtDNA release, leading to an increase in cytoplasmic mtDNA. GaELNs mitigated this effect, although the addition of NCT-503 attenuated protective impact of GaELNs, leading to increased mtDNA release (Figure 7J). Furthermore, we analyzed the expression of TOM20 and TFAM, key proteins involved in mitochondrial protein homeostasis and mtDNA synthesis. WB results indicated that LPS significantly downregulated TOM20 and TFAM expression, while GaELNs partially restored their levels. However, following NCT-503 addition, TOM20 and TFAM expression levels did not differ significantly from those seen with LPS alone (Figure 7K–M). These results suggest that GaELNs substantially ameliorate mitochondrial dysfunction under inflammatory conditions, a process closely associated with PHGDH/PI3K/AKT.

Discussion

Periodontitis is a chronic infectious disease of the periodontal tissues caused by dental plaque biofilms, which, once established, is irreversible and represents a significant global burden.⁴⁶ The application of local drug therapy is considered an important adjunct to mechanical debridement in the treatment of periodontitis; however, current drugs for periodontitis lack direct anti-inflammatory effects and the ability to promote tissue health restoration.⁴⁷ Therefore, the development of novel, locally applicable anti-inflammatory drugs hold significant promise. Traditional drug development, however, involves lengthy timelines and presents uncertainties in both safety and efficacy. Exosome-like nanovesicles derived from natural plant sources offer advantages such as low cost, high safety, broad action profiles, strong targeting capabilities and scalability for mass production, making them a rapidly expanding area of research and a burgeoning focus of interest.^{48,49} Among these, GaELNs possess potent anti-inflammatory and antioxidant properties and have been studied in conditions such as colitis, hepatitis and osteoarthritis, though their effects on periodontitis remain unexplored. In this study, we extracted GaELNs using an innovative and rapid physical method, revealing through multi-omics analysis that GaELNs contain numerous bioactive compounds capable of promoting cell proliferation through metabolic reprogramming, reducing pro-inflammatory cytokine secretion in LPS-stimulated cells, mitigating cellular oxidative stress and enhancing mitochondrial function. These effects ultimately contribute to mitigating tissue loss associated with periodontitis.

Metabolic reprogramming plays a pivotal role in various diseases, including cancer, immune disorders, tissue regeneration and infections, and is considered one of the most promising approaches for treating periodontitis.^{50–52} The excessive immune-inflammatory response of local periodontal tissues to bacterial LPS and similar stimuli is

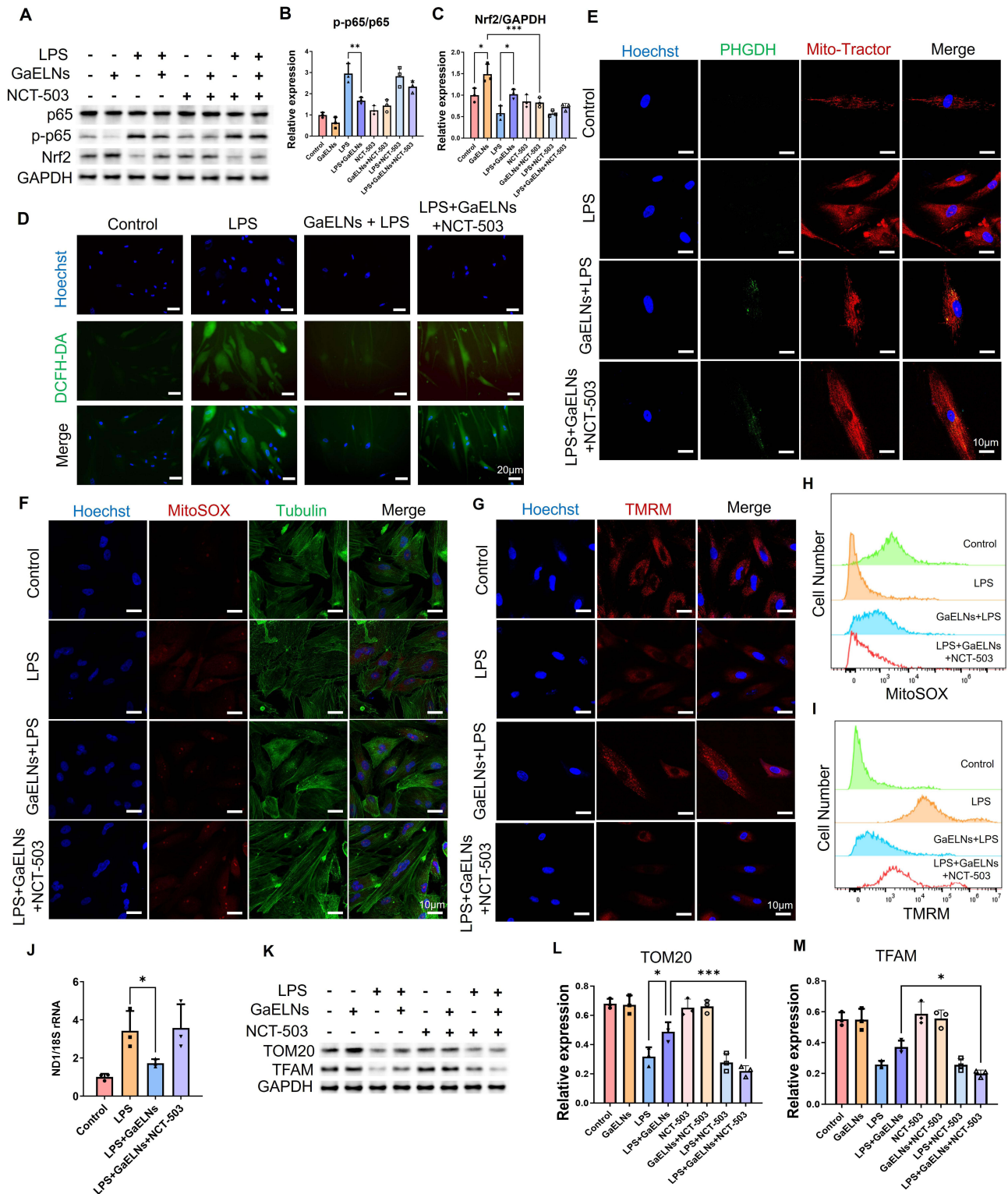


Figure 7 GaELNs Reduce Inflammation and Oxidative Stress and Improve Mitochondrial Function by Downregulating p65 and Upregulating Nrf2 via the PHGDH/PI3K/AKT Pathway. **(A)** WB analysis of p65, p-p65, Nrf2 and GAPDH expression levels in whole cell lysates. **(B and C)** Relative protein expression levels of p-p65/p65 and Nrf2/GAPDH based on band intensities (n=3). **(D)** DCFH-DA staining to assess intracellular ROS levels in HGF under different treatments. Scale bar = 20 μ m. **(E)** Immunofluorescence and Mito-Tractor staining to observe PHGDH expression and mitochondrial morphology in HGF following different treatments. Scale bar = 10 μ m. **(F)** MitoSOX fluorescence staining to measure mitochondrial ROS levels in HGF under different treatments. Scale bar = 10 μ m **(G)** TMRM fluorescence staining to assess mitochondrial membrane potential in HGF under different treatments. Scale bar = 10 μ m **(H)** Flow cytometry analysis of MitoSOX fluorescence intensity. **(I)** Flow cytometry analysis of TMRM fluorescence intensity. **(J)** Ratio of cytoplasmic ND1 to 18s rRNA levels (n=3). **(K)** WB analysis of TOM20, TFAM and GAPDH expression levels in whole cell lysates. **(L and M)** Relative protein expression levels of TOM20/GAPDH and TFAM/GAPDH based on band intensities (n=3). All data are expressed as mean \pm SD, *p < 0.05, **p < 0.01, ***p < 0.001, ****p < 0.0001.

a primary cause of periodontal tissue loss. During this process, inflammatory factors damage the mitochondrial electron transport chain, resulting in substantial ROS production.⁵³ As mitochondrial function is compromised, other intracellular energy metabolism pathways, such as glycolysis, become markedly upregulated to rapidly meet high energy demands. Concurrently, the pentose phosphate pathway (PPP) becomes more active to produce additional NADPH, helping to maintain redox balance in response to oxidative stress.⁵⁴ Excessive energy metabolism imbalance and ROS accumulation ultimately lead to cell death. Therefore, metabolic reprogramming aimed at restoring energy metabolism and reducing oxidative stress holds great therapeutic promise.⁵⁵ We observed that the introduction of GaELNs significantly upregulated PHGDH expression and further activated the PI3K/AKT pathway, with a strong correlation between PHGDH and PI3K/AKT expression, consistent with recent findings.⁴¹ PHGDH, a critical rate-limiting enzyme in serine synthesis, is essential for nucleotide, lipid and amino acid synthesis and for maintaining redox balance. Recent studies indicate that PHGDH can directly inhibit inflammatory responses by reducing M1 macrophages and promoting M2 macrophage differentiation via suppression of the p38-JAK-STAT1 pathway.⁴⁰ Additionally, the PI3K/AKT signaling pathway plays an essential role in metabolic reprogramming, exerting various biological functions through the regulation of distinct downstream signaling molecules. Our study demonstrated that co-culture with GaELNs markedly upregulated mTOR, VEGF and Nrf2, while significantly downregulating P65 expression. Activation of mTOR, a key step in PI3K/AKT-mediated metabolic reprogramming, promotes protein and lipid synthesis and regulates autophagy, which is vital for mitochondrial function and energy metabolism, ensuring sufficient energy supply under stress conditions.⁵⁶ VEGF, a crucial pro-angiogenic factor, not only promotes angiogenesis but also enhances cellular adaptation to stress environments by improving tissue oxygen metabolism.⁵⁷ Nrf2 is a central regulator of cellular antioxidant responses, upregulating various antioxidant enzymes, such as superoxide dismutase (SOD) and glutathione peroxidase (GPx), thereby enhancing the cell's ability to counteract oxidative stress.⁵⁸ In contrast, NF- κ B is a core regulatory molecule of pro-inflammatory factors and its inhibition can reduce the secretion of inflammatory cytokines, thereby alleviating inflammation.⁵⁹

Mitochondria play a central role in metabolic reprogramming, functioning not only as the hub of energy metabolism but also as the primary source of intracellular ROS. Under inflammatory conditions, mitochondrial fission increases, resulting in a fragmented, granular structure, with disrupted electron transport along the oxidative phosphorylation (OXPHOS) chain. This obstruction reduces proton reflow, lowers membrane potential and impairs ATP synthesis. When the electron transport chain is compromised, electrons leak and combine with oxygen to form superoxide, raising ROS levels.⁶⁰ Concurrently, decreased expression of TFAM and TOM20 disrupts mitochondrial DNA replication and normal mitochondrial protein translocation. Consequently, cells fail to produce sufficient ATP, ROS generation escalates and antioxidant capacity diminishes, leading to a state of oxidative stress.⁶¹ This, in turn, exacerbates mitochondrial damage in a vicious cycle that intensifies inflammation. Additionally, mtDNA released due to mitochondrial damage can directly drive the progression of inflammation. Extensive research has shown that mitochondrial dysfunction is closely linked to the pathogenesis and progression of periodontitis.⁶² Our findings indicate that the addition of GaELNs significantly ameliorates mitochondrial dysfunction, a process closely associated with PHGDH. PHGDH contributes to mitochondrial protein synthesis, NADPH production and glutathione-based antioxidant defenses, enhancing mitochondrial resistance to oxidative stress. Furthermore, the PI3K/AKT signaling pathway activated by PHGDH is crucial in regulating mitochondrial function. High Nrf2 expression and NF- κ B inhibition markedly reduce mitochondrial oxidative stress, decrease the abundance of damaged mtDNA and proteins, while AKT and mTOR promote the expression of TFAM and TOM20, regulating mitophagy and mitochondrial turnover to improve mitochondrial quality, function and stability. In summary, the diverse bioactive substances within GaELNs activate the PI3K/AKT pathway via PHGDH, suppressing cellular inflammation and oxidative stress through metabolic reprogramming, promoting mitochondrial function and cellular proliferation to restore periodontal health and support periodontal tissue regeneration.

However, several issues must be addressed before GaELNs can be applied in clinical settings, such as quality control and consistency across different varieties and sources of GaELNs, the establishment of systematic safety evaluation protocols and the current lack of extensive clinical studies. Nonetheless, we are confident that GaELNs hold significant promise and are poised to make a profound impact in the field of medicine.

Conclusion

In summary, this study demonstrates that GaELNs significantly enhance mitochondrial function, reduce inflammation and oxidative stress and promote cell proliferation by activating the PHGDH/PI3K/AKT signaling pathway. These effects ultimately lead to a reduction in bone resorption and tissue loss associated with periodontitis. As a novel and effective therapeutic strategy for periodontitis, GaELNs exhibit promising potential for clinical application.

Abbreviations

GaELNs, Garlic-Derived Exosome-Like Nanovesicles; HGF, Human Gingival Fibroblasts; LPS, Lipopolysaccharide; VEGF, Vascular Endothelial Growth Factor; CXCL, Chemokine (C-X-C Motif) Ligand; IL, Interleukin; ROS, Reactive Oxygen Species; CAT, Catalase; GSR, Glutathione Reductase; HO-1, Heme Oxygenase-1; NQO1, NAD(P)H Quinone Dehydrogenase 1; Nrf2, Nuclear Factor Erythroid 2-Related Factor 2; NF- κ B, Nuclear Factor Kappa B; PHGDH, Phosphoglycerate Dehydrogenase; PI3K, Phosphatidylinositol 3-Kinase; AKT, Protein Kinase B; mTOR, Mammalian Target of Rapamycin; TRAP, Tartrate-Resistant Acid Phosphatase; TNF- α , Tumor Necrosis Factor- α ; KEGG, Kyoto Encyclopedia of Genes and Genomes; GO, Gene Ontology; RPKM, Reads Per Kilobase Million; FDR: False Discovery Rate; qRT-PCR, Quantitative Real-Time Polymerase Chain Reaction; ELISA, Enzyme-Linked Immunosorbent Assay; DCFH-DA, Dichlorodihydrofluorescein Diacetate; TEM, Transmission Electron Microscopy; NTA, Nanoparticle Tracking Analysis; PAGE, Polyacrylamide Gel Electrophoresis; BCA, Bicinchoninic Acid; DIO, 3,3'-Diocadecyloxycarbocyanine Perchlorate; DAPI, 4',6-Diamidino-2-Phenylindole; DIL, 1,1'-Diocadecyl-3,3,3',3'-Tetramethylindocarbocyanine Perchlorate; CCK-8, Cell Counting Kit-8; EDTA, Ethylenediaminetetraacetic Acid; H&E, Hematoxylin and Eosin; Mito-Tracker, Mitochondrial Tracker; Mito-SOX, Mitochondrial Superoxide Indicator; TMRM, Tetramethylrhodamine Methyl Ester Perchlorate; ND1, NADH Dehydrogenase Subunit 1; ANOVA, Analysis of Variance; ICMJE, International Committee of Medical Journal Editors.

Acknowledgments

This research was supported by the National Key Research and Development Program of China (No. 2023YFC2506300) and the Nature Science Foundation of Beijing (No. 7244446).

Author Contributions

All authors made a significant contribution to the work reported, whether that is in the conception, study design, execution, acquisition of data, analysis and interpretation, or in all these areas; took part in drafting, revising or critically reviewing the article; gave final approval of the version to be published; have agreed on the journal to which the article has been submitted; and agree to be accountable for all aspects of the work.

Disclosure

The authors report no conflicts of interest in this work.

References

- Zhang L, Nie F, Zhao J, et al. PGRN is involved in macrophage M2 polarization regulation through TNFR2 in periodontitis. *J Transl Med.* 2024;22(1):407. doi:10.1186/s12967-024-05214-7
- Perez CM, Munoz F, Andriankaja OM, et al. Cross-sectional associations of impaired glucose metabolism measures with bleeding on probing and periodontitis. *J Clin Periodontol.* 2017;44(2):142–149. doi:10.1111/jcpe.12662
- Lee H, Joo JY, Song JM, Kim HJ, Kim YH, Park HR. Immunological link between periodontitis and type 2 diabetes deciphered by single-cell RNA analysis. *Clin Transl Med.* 2023;13(12):e1503. doi:10.1002/ctm2.1503
- Kondo T, Gleason A, Okawa H, Hokugo A, Nishimura I. Mouse gingival single-cell transcriptomic atlas identified a novel fibroblast subpopulation activated to guide oral barrier immunity in periodontitis. *Elife.* 2023;12. doi:10.7554/eLife.88183
- Liu A, Hayashi M, Ohsugi Y, et al. The IL-33/ST2 axis is protective against acute inflammation during the course of periodontitis. *Nat Commun.* 2024;15(1):2707. doi:10.1038/s41467-024-46746-2
- Wenjing S, Mengmeng L, Lingling S, Tian D, Wenyan K, Shaohua G. Galectin-3 inhibition alleviated LPS-induced periodontal inflammation in gingival fibroblasts and experimental periodontitis mice. *Clin Sci.* 2024;138(12):725–739. doi:10.1042/CS20240036
- Paladines N, Dawson S, Ryan W, et al. Metabolic reprogramming through mitochondrial biogenesis drives adenosine anti-inflammatory effects: new mechanism controlling gingival fibroblast hyper-inflammatory state. *Front Immunol.* 2023;14:1148216. doi:10.3389/fimmu.2023.1148216

8. Su W, Li J, Jiang L, Lei L, Li H. Hexokinase 2-mediated glycolysis supports inflammatory responses to *Porphyromonas gingivalis* in gingival fibroblasts. *BMC Oral Health*. 2023;23(1):103. doi:10.1186/s12903-023-02807-4
9. Yan Q, Shi S, Ge Y, Wan S, Li M, Li M. Nanoparticles of cerium-doped zeolitic imidazolate framework-8 promote soft tissue integration by reprogramming the metabolic pathways of macrophages. *ACS Biomater Sci Eng*. 2023;9(7):4241–4254. doi:10.1021/acsbomaterials.3c00508
10. Mukherjee A, Ghosh KK, Chakraborty S, Gulyas B, Padmanabhan P, Ball WB. Mitochondrial reactive oxygen species in infection and immunity. *Biomolecules*. 2024;14(6). doi:10.3390/biom14060670
11. Wang H, Peng Y, Huang X, et al. Glycometabolic reprogramming in cementoblasts: a vital target for enhancing cell mineralization. *FASEB J*. 2023;37(11):e23241. doi:10.1096/fj.202300870RR
12. Zhou J, Shi P, Ma R, Xie X, Zhao L, Wang J. Notopterol inhibits the NF-kappaB pathway and activates the PI3K/Akt/Nrf2 pathway in periodontal tissue. *J Immunol*. 2023;211(10):1516–1525. doi:10.4049/jimmunol.2200727
13. Wang W, Zhou Z, Ding T, et al. Capsaicin attenuates *Porphyromonas gingivalis*-suppressed osteogenesis of periodontal ligament stem cells via regulating mitochondrial function and activating PI3K/AKT/mTOR pathway. *J Periodontol Res*. 2024;59(4):798–811. doi:10.1111/jre.13252
14. Shen S, Sun T, Ding X, et al. The exoprotein Gbp of *Fusobacterium nucleatum* promotes THP-1 cell lipid deposition by binding to CypA and activating PI3K-AKT/MAPK/NF-kappaB pathways. *J Adv Res*. 2024;57:93–105. doi:10.1016/j.jare.2023.04.007
15. Lin SY, Sun JS, Lin IP, Hung MC, Chang JZ. Efficacy of adjunctive local periodontal treatment for type 2 diabetes mellitus patients with periodontitis: a systematic review and network meta-analysis. *J Dent*. 2024;148:105212. doi:10.1016/j.jdent.2024.105212
16. Rejabi A, Ram A, Nazari A, Arefnezhad R, Rezaei-Tazangi F. Does crocin create new hope for the treatment of oral problems? A focus on periodontitis. *Mol Biol Rep*. 2024;51(1):224. doi:10.1007/s11033-024-09209-x
17. Dad HA, Gu TW, Zhu AQ, Peng LH. Plant exosome-like nanovesicles: emerging therapeutics and drug delivery nanoplatfoms. *Mol Ther*. 2021;29(1):13–31. doi:10.1016/j.ymthe.2020.11.030
18. Sundaram K, Teng Y, Mu J, et al. Outer membrane vesicles released from garlic exosome-like nanoparticles (GaELNs) train gut bacteria that reverses type 2 diabetes via the gut-brain axis. *Small*. 2024;20(20):e2308680. doi:10.1002/sml.202308680
19. Zhao B, Lin H, Jiang X, et al. Exosome-like nanoparticles derived from fruits, vegetables, and herbs: innovative strategies of therapeutic and drug delivery. *Theranostics*. 2024;14(12):4598–4621. doi:10.7150/thno.97096
20. Bai C, Liu J, Zhang X, et al. Research status and challenges of plant-derived exosome-like nanoparticles. *Biomed Pharmacother*. 2024;174:116543. doi:10.1016/j.biopha.2024.116543
21. Langellotto MD, Rassu G, Serri C, Demartis S, Giunchedi P, Gavini E. Plant-derived extracellular vesicles: a synergetic combination of a drug delivery system and a source of natural bioactive compounds. *Drug Deliv Transl Res*. 2024. doi:10.1007/s13346-024-01698-4
22. Wei C, Zhang M, Cheng J, Tian J, Yang G, Jin Y. Plant-derived exosome-like nanoparticles - from Laboratory to factory, a landscape of application, challenges and prospects. *Crit Rev Food Sci Nutr*. 2024;1–19. doi:10.1080/10408398.2024.2388888
23. De Greef D, Barton EM, Sandberg EN, et al. Anticancer potential of garlic and its bioactive constituents: a systematic and comprehensive review. *Semin Cancer Biol*. 2021;73:219–264. doi:10.1016/j.semcancer.2020.11.020
24. Rouf R, Uddin SJ, Sarker DK, et al. Antiviral potential of garlic (*Allium sativum*) and its organosulfur compounds: a systematic update of pre-clinical and clinical data. *Trends Food Sci Technol*. 2020;104:219–234. doi:10.1016/j.tifs.2020.08.006
25. Yun HM, Ban JO, Park KR, et al. Potential therapeutic effects of functionally active compounds isolated from garlic. *Pharmacol Ther*. 2014;142(2):183–195. doi:10.1016/j.pharmthera.2013.12.005
26. Wang X, Liu Y, Dong X, et al. peu-MIR2916-p3-enriched garlic exosomes ameliorate murine colitis by reshaping gut microbiota, especially by boosting the anti-colicitid *Bacteroides thetaiotaomicron*. *Pharmacol Res*. 2024;200:107071. doi:10.1016/j.phrs.2024.107071
27. Liu J, Li W, Bian Y, et al. Garlic-derived exosomes regulate PFKFB3 expression to relieve liver dysfunction in high-fat diet-fed mice via macrophage-hepatocyte crosstalk. *Phytomedicine*. 2023;112:154679. doi:10.1016/j.phymed.2023.154679
28. Liu Y, Nie M, Li X, et al. Garlic-derived exosomes alleviate osteoarthritis through inhibiting the MAPK signaling pathway. *Appl Biochem Biotechnol*. 2024. doi:10.1007/s12010-024-05047-6
29. Bian Y, Li W, Jiang X, et al. Garlic-derived exosomes carrying miR-396e shapes macrophage metabolic reprogramming to mitigate the inflammatory response in obese adipose tissue. *J Nutr Biochem*. 2023;113:109249. doi:10.1016/j.jnutbio.2022.109249
30. Chabi M, Goulas E, Galinousky D, et al. Identification of new potential molecular actors related to fiber quality in flax through omics. *Front Plant Sci*. 2023;14:1204016. doi:10.3389/fpls.2023.1204016
31. Ahmad P, Shah A, Waiz M, Chaturvedi CP, Alvi SS, Khan MS. Organosulfur compounds, S-Allyl-L-Cysteine and S-Ethyl-L-Cysteine, Target PCSK-9/LDL-R-Axis to Ameliorate Cardiovascular, hepatic, and metabolic changes in high carbohydrate and high fat diet-induced metabolic syndrome in rats. *Phytother Res*. 2024. doi:10.1002/ptr.8323
32. Kouhi ZH, Seyedalipour B, Hosseinkhani S, Chaichi MJ. Bisdemethoxycurcumin, a novel potent polyphenolic compound, effectively inhibits the formation of amyloid aggregates in ALS-associated hSOD1 mutant (L38R). *Int J Biol Macromol*. 2024;282(Pt 2):136701. doi:10.1016/j.ijbiomac.2024.136701
33. Park W, Song G, Lim W, Park S. Therapeutic effects of S-allyl-L-cysteine in a mouse endometriosis model and its immunomodulatory effects via regulation of T cell subsets and cytokine expression. *Pharmacol Rep*. 2024;76(5):1089–1099. doi:10.1007/s43440-024-00625-1
34. Sung M, Lim S, Park S, Choi Y, Kim S. Anti-inflammatory effects of phytosphingosine-regulated cytokines and NF-kB and MAPK mechanism. *Cell mol Biol*. 2024;70(9):22–30. doi:10.14715/cmb/2024.70.9.3
35. Lee CM, Hwang Y, Kim M, Park YC, Kim H, Fang S. PHGDH: a novel therapeutic target in cancer. *Exp Mol Med*. 2024;56(7):1513–1522. doi:10.1038/s12276-024-01268-1
36. Yoon BK, Kim H, Oh TG, et al. PHGDH preserves one-carbon cycle to confer metabolic plasticity in chemoresistant gastric cancer during nutrient stress. *Proc Natl Acad Sci U S A*. 2023;120(21):e2217826120. doi:10.1073/pnas.2217826120
37. Hamano M, Haraguchi Y, Sayano T, et al. Enhanced vulnerability to oxidative stress and induction of inflammatory gene expression in 3-phosphoglycerate dehydrogenase-deficient fibroblasts. *FEBS Open Bio*. 2018;8(6):914–922. doi:10.1002/2211-5463.12429
38. Huang H, Liu K, Ou H, Qian X, Wan J. Phgdh serves a protective role in Il-1beta induced chondrocyte inflammation and oxidative-stress damage. *Mol Med Rep*. 2021;23(6). doi:10.3892/mmr.2021.12058
39. Wang C, Zhao M, Bin P, et al. Serine synthesis controls mitochondrial biogenesis in macrophages. *Sci Adv*. 2024;10(20):eadn2867. doi:10.1126/sciadv.adn2867

40. Shan X, Hu P, Ni L, et al. Serine metabolism orchestrates macrophage polarization by regulating the IGF1-p38 axis. *Cell mol Immunol.* 2022;19(11):1263–1278. doi:10.1038/s41423-022-00925-7
41. Cai Z, Li W, Hager S, et al. Targeting PHGDH reverses the immunosuppressive phenotype of tumor-associated macrophages through alpha-ketoglutarate and mTORC1 signaling. *Cell mol Immunol.* 2024;21(5):448–465. doi:10.1038/s41423-024-01134-0
42. Ma X, Li B, Liu J, Fu Y, Luo Y. Phosphoglycerate dehydrogenase promotes pancreatic cancer development by interacting with eIF4A1 and eIF4E. *J Exp Clin Cancer Res.* 2019;38(1):66. doi:10.1186/s13046-019-1053-y
43. Dini A, Barker H, Piki E, et al. A multiplex single-cell RNA-Seq pharmacotranscriptomics pipeline for drug discovery. *Nat Chem Biol.* 2024;21:432–442. doi:10.1038/s41589-024-01761-8
44. Wen X, Tang S, Wan F, Zhong R, Chen L, Zhang H. The PI3K/Akt-Nrf2 signaling pathway and mitophagy synergistically mediate hydroxytyrosol to alleviate intestinal oxidative damage. *Int J Biol Sci.* 2024;20(11):4258–4276. doi:10.7150/ijbs.97263
45. Zhao F, Piao J, Song J, et al. Traditional Chinese Herbal Formula, fuzi-lizhong pill, produces antidepressant-like effects in chronic restraint stress mice through systemic pharmacology. *J Ethnopharmacol.* 2025;338:119011. doi:10.1016/j.jep.2024.119011
46. Bai Y, Guo HL, Hua T, et al. Time-responsive activity of engineered bacteria for local sterilization and biofilm removal in periodontitis. *Adv Healthc Mater.* 2024;14:e2401190. doi:10.1002/adhm.202401190
47. Graziani F, Karapetsa D, Alonso B, Herrera D. Nonsurgical and surgical treatment of periodontitis: how many options for one disease? *Periodontol.* 2017;75(1):152–188. doi:10.1111/prd.12201
48. Cao M, Diao N, Cai X, et al. Plant exosome nanovesicles (PENs): green delivery platforms. *Mater Horiz.* 2023;10(10):3879–3894. doi:10.1039/d3mh01030a
49. Mu N, Li J, Zeng L, et al. Plant-derived exosome-like nanovesicles: current progress and prospects. *Int J Nanomed.* 2023;18:4987–5009. doi:10.2147/IJN.S420748
50. Horn P, Tacke F. Metabolic reprogramming in liver fibrosis. *Cell Metab.* 2024;36(7):1439–1455. doi:10.1016/j.cmet.2024.05.003
51. Xiao J, Wang S, Chen L, et al. 25-Hydroxycholesterol regulates lysosome AMP kinase activation and metabolic reprogramming to educate immunosuppressive macrophages. *Immunity.* 2024;57(5):1087–1104e7. doi:10.1016/j.immuni.2024.03.021
52. Zebrowitz E, Aslanukov A, Kajikawa T, et al. Prolyl-hydroxylase inhibitor-induced regeneration of alveolar bone and soft tissue in a mouse model of periodontitis through metabolic reprogramming. *Front Dent Med.* 2022;3. doi:10.3389/fdmed.2022.992722
53. Luo S, Xu T, Zheng Q, et al. Mitochondria: an Emerging Unavoidable Link in the Pathogenesis of Periodontitis Caused by Porphyromonas gingivalis. *Int J mol Sci.* 2024;25(2). doi:10.3390/ijms25020737
54. Deng Y, Xiao J, Ma L, et al. Mitochondrial dysfunction in periodontitis and associated systemic diseases: implications for pathomechanisms and therapeutic strategies. *Int J mol Sci.* 2024;25(2). doi:10.3390/ijms25021024
55. Jiang W, Wang Y, Cao Z, et al. The role of mitochondrial dysfunction in periodontitis: from mechanisms to therapeutic strategy. *J Periodontol Res.* 2023;58(5):853–863. doi:10.1111/jre.13152
56. Li Y, Zhou Y, Liu D, et al. Glutathione Peroxidase 3 induced mitochondria-mediated apoptosis via AMPK /ERK1/2 pathway and resisted autophagy-related ferroptosis via AMPK/mTOR pathway in hyperplastic prostate. *J Transl Med.* 2023;21(1):575. doi:10.1186/s12967-023-04432-9
57. Xu X, Ye X, Zhu M, Zhang Q, Li X, Yan J. FtMt reduces oxidative stress-induced trophoblast cell dysfunction via the HIF-1alpha/VEGF signaling pathway. *BMC Pregnancy Childbirth.* 2023;23(1):131. doi:10.1186/s12884-023-05448-1
58. Yang T, Qu X, Zhao J, et al. Macrophage PTEN controls STING-induced inflammation and necroptosis through NICD/NRF2 signaling in APAP-induced liver injury. *Cell Commun Signal.* 2023;21(1):160. doi:10.1186/s12964-023-01175-4
59. Franz S, Ertel A, Engel KM, Simon JC, Saalbach A. Overexpression of S100A9 in obesity impairs macrophage differentiation via TLR4-NFkB-signaling worsening inflammation and wound healing. *Theranostics.* 2022;12(4):1659–1682. doi:10.7150/thno.67174
60. Andrieux P, Chevillard C, Cunha-Neto E, Nunes JPS. Mitochondria as a cellular hub in infection and inflammation. *Int J mol Sci.* 2021;22(21). doi:10.3390/ijms222111338
61. Liu H, Zhu S, Han W, Cai Y, Liu C. DMEP induces mitochondrial damage regulated by inhibiting Nrf2 and SIRT1/PGC-1alpha signaling pathways in HepG2 cells. *Ecotoxicol Environ Saf.* 2021;221:112449. doi:10.1016/j.ecoenv.2021.112449
62. Liu J, Wang Y, Shi Q, et al. Mitochondrial DNA efflux maintained in gingival fibroblasts of patients with periodontitis through ROS/mPTP pathway. *Oxid Med Cell Longev.* 2022;2022:1000213. doi:10.1155/2022/1000213

International Journal of Nanomedicine

Publish your work in this journal

The International Journal of Nanomedicine is an international, peer-reviewed journal focusing on the application of nanotechnology in diagnostics, therapeutics, and drug delivery systems throughout the biomedical field. This journal is indexed on PubMed Central, MedLine, CAS, SciSearch®, Current Contents®/Clinical Medicine, Journal Citation Reports/Science Edition, EMBASE, Scopus and the Elsevier Bibliographic databases. The manuscript management system is completely online and includes a very quick and fair peer-review system, which is all easy to use. Visit <http://www.dovepress.com/testimonials.php> to read real quotes from published authors.

Submit your manuscript here: <https://www.dovepress.com/international-journal-of-nanomedicine-journal>

Dovepress
Taylor & Francis Group